Paleomagnetism of ca. 750 Ma Syenite Dykes of the Southern Congo Craton, Northern Namibia

Seamus M.B. Houlihan
Prof. David A.D. Evans and Prof. Mark T. Brandon
1 May 2019

A Senior Thesis presented to the faculty of the Department of Geology and Geophysics, Yale University, in partial fulfillment of the Bachelor's Degree.

TABLE OF CONTENTS

ABSTRACT

In seeking to further the understanding of the motion of the Congo craton prior to its Cambrian consolidation within the Gondwana continent, this project analyzed thermal demagnetization of paleomagnetic samples from 21 quality-filtered sites in northern Namibia on the southern edge of the Congo craton, so that a more accurate location for the Congo craton at ca. 750 Ma can be incorporated into reconstructions of supercontinent Rodinia. No sites agree with the expected directions for the southern Congo at ca. 750 Ma, from previously published studies in the eastern side of the craton. Of the 21 sites, six are interpreted to carry present field directions due to a combination of weathering and/or viscous relaxation of multidomain magnetite. Four sites show a direction similar to early/middle Cambrian poles from Gondwana, including one site with visible sulfide mineralization. Of the remaining 11 sites, one carries a hematitic direction with is in the vicinity of a pole of unknown age from the eastern part of the craton which is associated with secondary hematite alteration; the other 10 sites have a streak distribution between expected late Ediacaran poles from the craton and a steep two-polarity direction, interpreted to have a slightly older age. Although the age of the steep remanence cannot be determined, three factors support the Cambrian overprint: the polar latitude implied by the pole is in contrast with the carbonate platform developed on the Congo craton at that time, it is notably distinct from previous 750 Ma Congo poles, and this direction is observed in both the dykes and basement thus suggesting a widespread thermochemical overprint. A paleomagnetic pole calculated from the 7 steepest sites suggests a polar excursion of the craton in mid-Ediacaran time. Given the extensive overprinting and remagnetization across the northern Damara foreland, this region proves unlikely to yield primary Precambrian poles.

INTRODUCTION

The formation of the supercontinent Gondwana occurred around 500 Ma (Gray *et al* 2008). This was the result of the collision of several major cratons, including the Congo and Kalahari (Gray *et al* 2008). These cratons are masses of continental crust which last collided about 500Ma. The orientation of the Congo and Kalahari cratons from 500 Ma is preserved today (Gray *et al* 2008). The country of Namibia includes the Kalahari and Congo cratons. However, the precise details of their collision and their locations before this time are not known. This research aims to provide more data about the Congo craton after 1100Ma, but prior to the final collision.

The collision resulted in the closure of the Khomas seaway and the Damara orogeny. The geologic remains of this collision are known as the Damara Belt. This project seeks to further the understanding of the motion of the Congo craton and the formation of the Damara Belt and to obtain a more accurate location for the Congo craton at 750Ma. This can be incorporated into reconstructions of the breakup of the supercontinent Rodinia. This project attempts to determine a new pole for the Congo craton at 750Ma; which could be then compared to poles from the Kalahari craton in a similar time period, to determine possible constraints on the size of the basin.

GEOLOGIC BACKGROUND

The samples were from the Welwitschia area of northern Namibia. This area is underlain by the Huab Basement complex, a collection of basement material of various ages and mineralizations (Frets 1969). This material is generally heavily metamorphized granites and schists (Frets 1969). The samples were taken from the dykes from the Oas syenite, a member of the Naauwpoort volcanics (Frets 1969). The Oas syenite is an intrusive quartz body with a coarse-grained texture and occasional phenocrysts (Frets 1969). The magnetite and hematite content of this body allowed for thermal demagnetization. The Oas syenite was dated at 751±6 Ma by Paul

Hoffman *et al.* in 1996. As shown in Figure 1, the Naauwpoort formation is overlain by two pairs of glaicgenic dimictite and warm-water carbonates—the combination of which evidence of Snowball Earth-style glaciation (Hoffman 2011). There is further carbonate material, the Tsumeb formation, which supports warm location for the craton during the Damara orogen (Hoffman and Halverson, 2008). The tectonic activity of the Damara orogen, which resulted in the suturing of the Congo and Kalahari cratons, occurred between 550 and 510 Ma(Gray *et al.* 2008). This tectonic activity could provide the energy for regional overprinting and remagnetization during this same window.

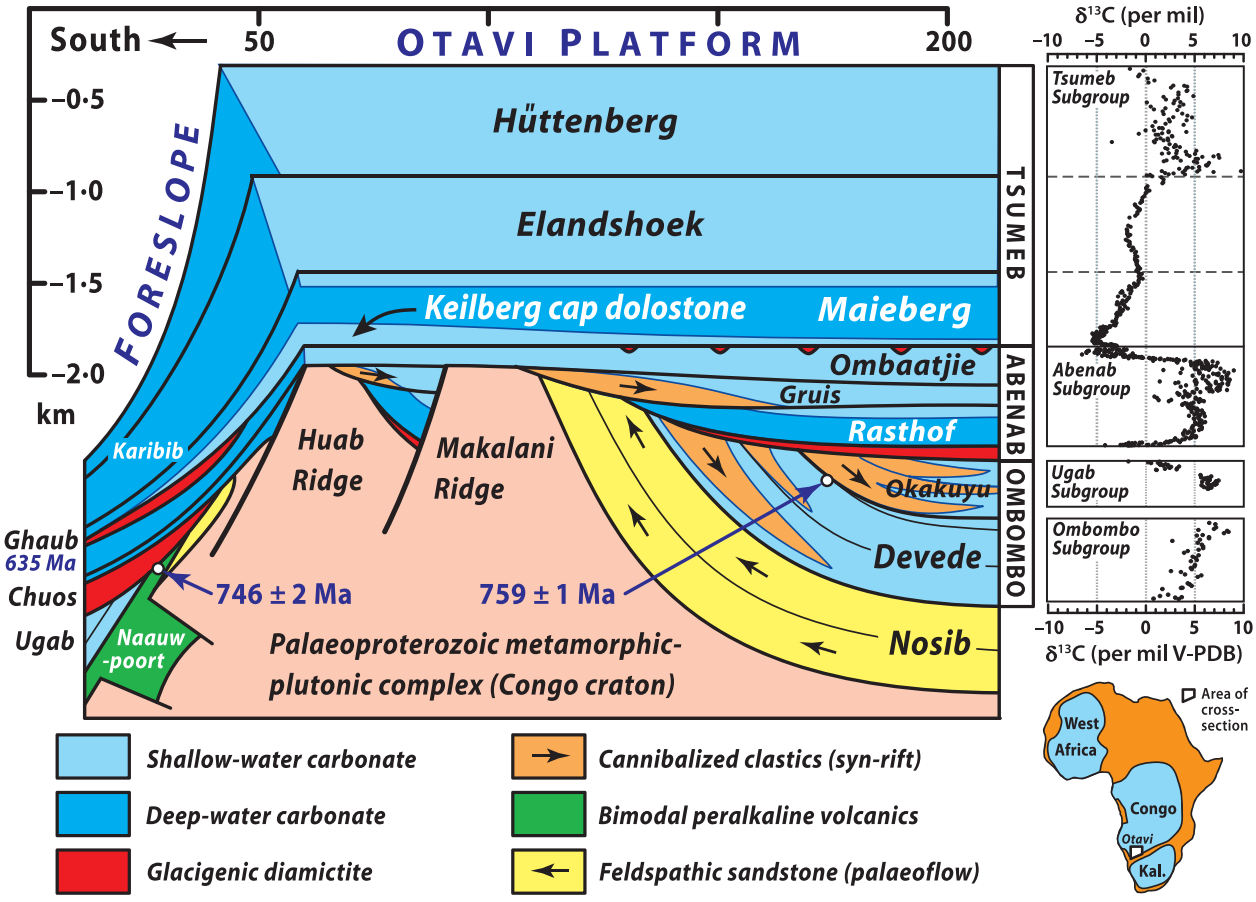

Figure 1: This figure summarizes the geologic environment of the Otavi Platform of the southern Congo craton. The carbonates overlay the material used for this study: dykes from the Oas syenite, a member of the Naauwpoort formation. (From Hoffman 2011).

METHODS

The 314 samples were collected by Prof. David Evans of Yale University, Prof. Johanna Salminen of University of Helsinki, and Prof. Ricardo Trindade of University of São Paulo in 2018; and by Prof. Evans, Emily Stewart of Yale University, and Seamus Houlihan in 2016. Sampling locations were previously identified as probable dykes using Google Earth satellite imagery, and routes to the dykes were obtained by mapping tracks on the same satellite images.

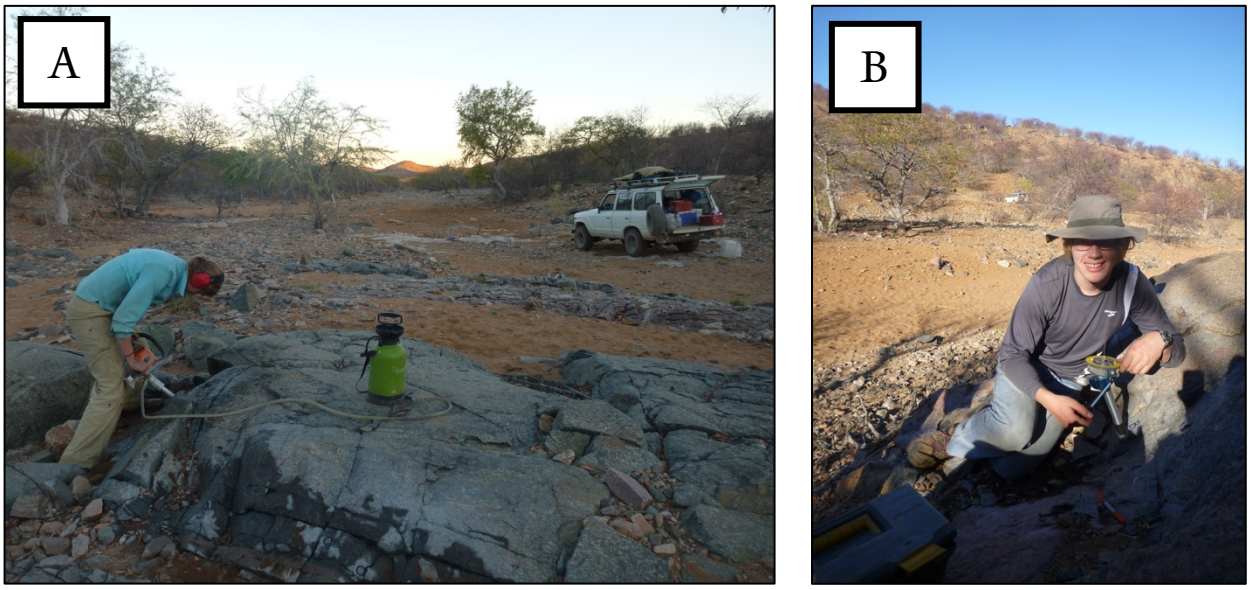

Figure 2: A. This photograph shows sample collection using a gasoline-powered paleomagnetic drill with attached water pump. Emily Stewart collects samples in 2016 at site H1607. **B.** This photograph is of Seamus Houlihan orienting samples using a combination sun- and magnetic-compass. Orientation would be carefully recorded and the sample marked to preserve the original orientation. Both photographs from David Evans.

Samples were collected in groups of 8 to 12 from a single rock unit, referred to as a site. Thirty-five sites were sampled. The samples were collected using a portable gasoline-powered paleomagnetic drill, with each sample being ideally longer than 5 cm. The orientation of each sample was recorded using an orientation device consisting of a solar compass, a Brunton magnetic compass, and a clinometer, as shown in Figure 2.

Upon returning to Kline Geology Lab at Yale University, the samples were cut to an approximate height of 1 cm using a dual-blade paleomagnetic rock saw. The central part of each

sample was used for the measurement. The front and end pieces were retained for possible mineralogical or geochemical analysis (not included in this study). Any samples which had cracked or broken were glued together using sodium silicate liquid as adhesive. The orientation information of each sample was recorded in an Excel header file, along with general information about each site. In two cases, samples were taken from the same dyke at different distances from a crosscutting dyke. This allowed two baked-contact tests to be performed. A baked-contact test compares the magnetic directions from the host rock to that of the intruding dykes. Samples were taken at various distances from the intruding dykes in the host rock. This allowed for the later comparison of the material between the two locations, as well as at distances in between (Buchan, 2007).

The Yale Paleomagnetic Facility was used for all paleomagnetic measurements. All measurements were taken within the facility's magnetic shield which reduces the local strength of Earth's magnetic field to less than 300 nT (nano-Telsa). A cryogenic DC-SQuID magnetometer with automatic sample changer was used to measure magnetic remanence. The natural remnant magnetization (NRM) of each sample was measured first. Then samples were submerged in liquid nitrogen and allowed to warm to room temperature. The magnetic moment was recorded again. Samples were then heated in 50ºC steps from 100ºC using a shielded ASC furnace, and measured at room temperature following each heating cycle. As the temperatures approached the Curie temperature for magnetite (580ºC), the temperature steps decreased in magnitude. Samples which may contain hematite were heated up to 675ºC, the Curie point of hematite.

After heating, the magnetic directions of the samples were analyzed to determine the components of magnetization. The Zijderveld diagram of each sample was compared with the

equal-area stereoplot to determine the number and direction of each component of magnetization. This process was accomplished using Craig Jones' PaleoMag software (Jones, 2002).

These components were named and identified by their behavior and likely mineralogical origin. These components were described sample by sample and averaged by site. Several different components were observed in the demagnetization of these samples, these components were used to describe different behaviors in the demagnetization process. Each sample had a liquid nitrogen (LN2) step, which defines the direction between the natural resonant magnetization measurement and the liquid nitrogen measurement. This component necessarily contains the natural resonant magnetization and liquid nitrogen measurements, and may contain any other measurements which are in the same direction of the natural resonant magnetization and liquid nitrogen. A goethite component (GOE) was observed in some samples and is a component describing the demagnetization between the 100ºC and the 300ºC steps. A pyrrhotite component (PYR) can also be described using the same temperature steps: since both pyrrhotite and goethite have an unblocking temperature between 300 and 350ºC, the names are based on the lithology of the site and the sample. A consistent direction which extends beyond the unblocking temperatures of pyrrhotite and goethite is summarized using a low temperature component (LTH). Low temperature components generally range from 200 to 500ºC. Beyond a low temperature component, a mid-temperature component is used to capture components with a higher ending temperature, between 500 and 600ºC. These components are useful in understanding the magnetic history of the sample, but often do not describe the oldest magnetic direction recorded by the sample.

As a sample thermally demagnetizes, it's behavior rapidly becomes unstable. This occurs once it passes beyond the highest unblocking temperature of any mineral contained in the sample. Once this occurs, the observed direction is secondarily derived from the ambient field of the heating ovens in the lab. These measurements are not useful in calculating a paleopole. The goal of separating the final components is to best approximate the characteristic component—a component which captures the oldest paleomagnetic signal of the sample. There are a variety of different behaviors which can be exhibited by a sample as it decreases in magnetism. The clearest is a signal to the origin. In this case, the strength of the magnetic moment decreases as the direction remains the same. This creates a clear line to the origin. A signal "to-the-origin" is also described by the mineral thought to be primarily responsible for the magnetic signal. Samples with an observed loss of magnetism between 580 and 600ºC, magnetite is assumed to the be the primary magnetic signal and for samples with a loss of magnetism near 670ºC, hematite. These characteristic components are referred to as magnetite to the origin (MTO) and hematite to the origin (HTO) respectively. In some cases, both minerals are thought to contribute to the component in which case it is named all to the origin (ATO). In all cases, the component is a line which includes and is anchored to the origin. It is possible for the measurements to cluster at single direction and not move towards the origin until the sample dies. These endpoints are formed of three or more points located in a similar location on the orthographic Zijderveld diagram. These stable endpoint components follow a similar naming convention to the origin characteristic components: magnetic endpoint (MEP), hematite endpoint (HEP), and stable endpoint (SEP). These components also include and are anchored to the origin. When the last points of the dying sample clearly does not intersect the origin a plane is required to capture the final component. The

plane must include the two components immediately preceding, as this would force the plane to include to the true characteristic component. This plane is referred to as a high plane (HPL), without regard to the possible mineralogical origin. These characteristic directions for each sample was determined using the final component of magnetization. These components were averaged using Fisher statistics to yield a characteristic direction for each site.

RESULTS

Following the site descriptions are stereo nets and Zijderveld diagrams for each site detailing the nature of the demagnetization and the characteristic component. Due to pervasive scatter and large error at both the site and sample level, sites H1604 and 13-20 are removed from analysis. These samples were fully demagnetized but are not included in this summary.

Site H1801 This site is a fine syenite dyke with a porphyritic texture. It is undulose and not more than 3 m wide. Most samples become unstable after heating beyond 400ºC, apart from samples F-I, which appear to have a strong hematite component. For the samples with hematite, they have a hematite end point, which gives a single direction after 400ºC. This site yields scattered results. Sample H1801E was removed from the analysis, as it was highly scattered overall. Samples A-D were removed from the final mean as they did not have clear characteristic components. The scattered results after 400ºC and the strong hematite, which is thought to be secondary, support possible overprinting at this site.

Site H1802 This site has two distinct groups of samples: a steeply upward group (A-E) and a downward western group (F-J). These two groups have distinct directions throughout measurement. In the first group (A-E) the LN2 direction is nearly parallel to the characteristic direction; both are southward and steeply upward. These five samples all show a clear goethite

component between 100ºC and 300ºC. These components were individually steeper (by ~20º) and trend slightly SSW. The characteristic direction is a clear and consistent direction to the origin with low error. In the second group (F-J), the three observed components have similar westerly declination. The observed goethite component has a shallower inclination. There is more error in the goethite components of the second group when compared to other measurements. Due to the scattered and low number of samples in each group, the $\alpha 95$ values for both groups are rather high (>20º).

Site H1803 Samples A-C are from fine-grained margin and do not have phenocrysts, D-J are more interior within the dyke and show phenocrysts up to 3cm. This site shows seven samples (D-J) with a strong characteristic component of magnetization. In each case, the magnetite to origin (MTO) direction is characteristic. There is often an irregular and nonlinear component between the LN2 and the MTO directions, which may represent the overlap of these components. A goethite component is sometimes located midway between the MTO and LN2 components, roughly downward and northwest. The characteristic component is steeper and more northward than the LN2. This characteristic component is very tightly clustered. After removing the pyrrhotite component the samples become unstable. The samples D-J seem to be affected by lightening due to a large demagnetization after the LN2 step, and are excluded from further analysis. This site shows likely pervasive overprinting from 500-525 Mya, based on a direction from sulfites within the Otavi carbonates with a similar direction suspected from the Damara belt, and therefore not used in the analysis Evans, D., personal comm., 2019). The smaller-grained samples A-C likely do not contain multi-domain magnetite, as they do not show the strong

lightening influence present in the other samples, and preserve an older, though not primary, magnetic direction.

Site H1804 This site showed clear three component systems (LN2, GOE, and MTO). Samples H, I, and J have weaker magnetic signals than the others, often yielding large errors. In these samples there was a possibility of another component between the GOE and MTO components. This is likely due to the overlap of these components. The magnetite-to-origin is characteristic and is more tightly clustered than the other components: it yields a steep northly down direction.

Site H1805 This site showed a large range of LN2 directions which condensed into a steeply downward characteristic direction. In the six samples where intermediate (5 of 6 were GOE, one LTH) directions were present, they had a similar declination but a much shallower inclination. These directions usually included steps from 200ºC to 350ºC. Across these five samples, GOE directions did not agree with each other to form a reliable direction. Between the intermediate and characteristic directions there was in each sample a large drop in the magnetic strength. After this drop the magnetite direction would lead into the origin in nine of ten cases. Sample G fails to stabilize at high temperature and does not yield final direction. The mid-temperature steps show motion towards the southward direction of 2 of the other samples. As it lacks a strong magnetite to origin component, the mid-temperature component will be used as a characteristic component.

Site H1806 This site showed a cross-cutting relationship with site H1807 and H1808. The LN2 mean of the site was steeply northeast and down and is the mean of a bimodal distribution. Few sample poles fall within the ellipse. A goethite direction was measured in 4 samples between 100ºC and 250ºC. This pole is northwest and up which agrees, for the most part, with the expected direction of this site. The pole is slightly more northeasterly than expected. This is

possibly due to an overlap with the LN2 or the characteristic direction. The characteristic direction is observed from the unblocking of magnetite. The steep northeast-down direction aligns closely with the LN2 for the site. This site has a low error and is used in analysis.

Site H1807 This site shows two-component magnetization with a noticeably overlap between components leading to a curve in the Zijderveld diagram between the LN2 direction and the characteristic direction. The LN2 component is equatorial and northeastern. The LN2 component is based on the natural resonant magnetization and the liquid nitrogen measurement, as the low temperature steps form a curve due to the overlap with the characteristic magnetization. Through demagnetization, the samples direction migrates from equatorial northeast to a characteristic direction of southwest and down. There is only one sample which disagrees with this direction (B), which yields a direction similar to the initial direction which is, coincidentally, the same as the reversal of the characteristic component.

Site H1808 This site was tightly clustered around an upward and north direction. The sample agree on both an LN2 and characteristic direction. The majority of the samples have a single component of magnetization and the direction is stable from LN2 until ~580ºC including and being forced through the origin. This site is the older of two dykes in a cross-cutting relationship, with H1806 and H1807. This site has a similar direction to these other sites.

Site H1809 This site shows a consistent shallow upward and northwestern pole in the LN2 and characteristic directions. There is also a goethite component visible in some samples between 100ºC and 250ºC. While an effect of this component was observed to extend to the Curie point of goethite (330ºC), the 300ºC was often not used in the fitting of the line due to overlap of this component with the adjacent component. This was observed as a smooth curve on the Zijderveld

plot of samples with a GOE component. In two samples (B and C) a goethite component was not observed, instead a pyrrhotite component at a slightly higher temperature is observed. These two sites show a direction consistent with a Cambrian sulfide overprint and are excluded from the GOE mean direction to form another mean direction. The GOE, LN2 and characteristic component has a similar declination to that of the characteristic direction, but a shallow inclination: Fisher ellipse is equatorial. In most cases, the 3 observed components were similar in declination and inclination. H stabilizes at a south and shallow MTO, which is not in agreement with the rest of the samples sites and is excluded from this analysis. Sample J shows magnetic stability after 580ºC, betraying the presence of hematite within the sample. The mid-temperature direction for this sample does not agree with any of the other directions, however there is a hematite endpoint observed on the orthographic diagram which provides a northwest and upward direction. This site is excluded from the analysis due to its similarity to the present dipole field.

Site H1810 This site showed a clear characteristic direction. The LN2 direction was usually parallel to the characteristic direction. In several cases there was a single component of magnetization was observed, the characteristic direction included the LN2 and NRM measurements. In these cases, an LN2 component and MTO component were recorded so they could be viewed in context in least squares equal area diagrams. The direction obtained was to upward and to the northeast. In four samples a lower temperature component was observed, ranging from 150ºC to 450ºC. This component was slightly shallower but with the same declination as the characteristic component. Sample G is excluded as its characteristic direction is far out of agreement with those of the rest of the samples.

Site H1811 This is a porphyritic potassium feldspar dyke. Samples E-K of this site show a consistent loss of magnetic moment between the 300 and 400ºC steps. After losing the majority of their magnetic moment, samples retain a direction nearly parallel to that of the LN2 direction. In a few cases, there is a goethite direction which is slightly steeper than that of the LN2 and characteristic directions. The first four samples (A-D) do not show a consistent direction. Their directions are usually shallow, but are unable to be resolved. Samples H-J show evidence of remagnetization due to lightning strike, and are not included in this analysis. Large scale remagnetization is likely due to the parallel relationship between the components.

Site H1812 This site's ten samples have a mean LN2 direction of northwest-up with a wide scattering of lines. There is a goethite component observed in six of the ten sites which provides a similar direction to the LN2. A low temperature component was observed in four samples (three of which had also shown a clear goethite component): this direction was steeply up. The low-temperature component was observed in these samples between 300ºC and 500ºC. As the temperature of demagnetization increases the directions trend from west to east concluding with the characteristic direction: steeply upward with a slight eastward trend. While all the characteristic directions are upward, they are otherwise scattered in various directions. Samples A, F, G, and H are excluded as they are scattered from the primary direction.

Site H1813 This site shows a consistent LN2 and MTO/ATO direction. In most cases, an overlap between the components leads to a curve in the orthographic Zijderveld diagram. The points within the curve were ignored in the least-squares analysis. The least-squares analysis shows a clear up and northwest direction for the characteristic direction. This is measurement includes linear components for nine of the ten samples and a plane for the tenth sample. Most samples

required heating to 625ºC until the magnetic signal was lost. The samples likely contain both magnetite and hematite. The hematite is likely secondary due to the presence of hematitic signaling and the strong northwest and up direction is near a middle Cambrian direction for this location on the craton.

Site H1814 This site shows a consistent upward and north-west direction. The LN2 are more scattered around than the mean than those of the characteristic direction. In the LN2 direction only one of the samples occurring within the Fisher ellipse, with directions scattered throughout the upward and NW region. The characteristic direction was more densely arranged, NNW and upward. The characteristic directions were based on temperature steps from 150ºC to 580ºC and all samples have a single component of magnetization after the liquid nitrogen step. This is an all to origin (ATO) magnetic signal. The steeply upward north signal in 9 of the ten samples is likely secondary due to high levels of weathering at the site. These samples show a streaky distribution leading to the tenth sample, I, is very possibly the most reliable. Most samples show hematite development, especially those best described with and ATO signal. This is evidence for possible remagnetization of these samples.

Site H1815 This site shows a consistent north and upward directions. As the temperature increases towards the unblocking temperature of magnetite, the direction moves from an LN2 direction of NNE to a characteristic direction of NNW. A goethite component is observed in 7 samples between 150ºC and 350ºC. There is a low temperature component in 4 of the samples, 3 of which also have a goethite component. This direction is between the characteristic (magnetite-to-origin) direction and the goethite component, possibly due to overlapping remnant directions. The characteristic is the most tightly clustered direction.

Site H1601 This site shows a single strong component of magnetization from the NRM step until temperatures above 600ºC. Samples show a slight amount of scatter between 150º and 350ºC, possibly due to goethite or pyrrhotite, but no strong component is measurable. These ATO directions are used to determine the characteristic direction of downward and NNW.

Site H1602 This site shows a single strong component of magnetization. The LN2 direction and the characteristic directions are very similar. However, they are separated by several measurements (150ºC to 350ºC) which to not yield any sense of direction or a possible line of best fine in a least square analysis. This messy segment is not present in two samples of the seven (B and G). The characteristic direction is slightly upward and west-southwest.

Site H1603 This site has consistent steeply upward direction. The LN2 unblocking direction and the magnetite to origin direction were not parallel. The characteristic direction was the only other component of magnetization in all cases, with the MTO component extending from 150ºC to 580ºC. The demagnetization is smooth and does not show a goethite component. Due to the general lack of agreement of the directions, this site was not used in the analysis.

Site H1605 This site showed two components of magnetization: an LN2 unblocking and an magnetite to origin component. While the LN2 unblocking directions are more scattered than the characteristic MTO direction, they yield a similar pole. Both yield a generally steep downward direction. Two samples are yield directions equatorial and east in both the LN2 and MTO components: these are far out of agreement with the others.

Site H1606 This site shows a two-component system A substantial LN2 component which is nearly parallel to the characteristic component, and the characteristic component. The large NRM to LN2 steps comprise the LN2 components and represent significant loss of magnetic moment.

The characteristic component shows a gradual loss of magnetic strength as it moves slowly towards the origin. The characteristic component is tightly clustered in a steeply upward direction. Two of the 8 samples are removed from the analysis as they are equatorial and not in agreement with the site mean.

Site H1607 While each sample shows a general eastward and southward drift, there is little to no agreement between samples and does not create a conclusive pole. The thermomagnetic curve (J/J0 diagram) shows a smooth transition from NRM to the origin, with samples lacking a "shoulder" of demagnetization. Samples showed an overlap between the LN2 and characteristic directions leading to a slight curve of the Zijderveld diagram between 150ºC and 300ºC. Due to a lack of agreement between samples this site is not included in this analysis.

Site H1608 The ten samples of this site all have a LN2 direction of steeply upward. This direction slowly moves toward the southeast. There is a low temperature component (LTH) in 3 samples, however the results to not agree to form a reliable pole: 2 are NW and up while the third is north and down. Four of the sites do not resolve to the origin and are best described as planes including the origin. These four planes indicate a very different direction than that of the magnetite-to-origin (MTO) direction from the other 8 samples. The MTO directions average to a steeply upward southeastern direction while the planes yield an equatorial east.

Site H1609 This site yielded a single characteristic direction beyond the LN2 unblocking. The LN2 unblocking was clearly distinct from that of the magnetite-to-origin direction, except in one sample where there was only one component. The LN2 unblocking often extended to the 100 or 150ºC step. In the other seven samples, the steps between 150ºC and 300ºC were often messier? than the following samples, while being part of the same component.

Site H1610 This site was a baked contact test with the sampled material was host rock. The samples getting progressively further from the dyke. This yielded two distinct groups: samples A-F and L-Q. The first subset (A-F) had a single component of magnetization and an upward and north direction. This is likely the result of remagnetization as the direction is very similar to the present dipole field. The second subset (L-Q) yielded dual-polarity characteristic directions, steeply upward southwest and steeply downward northeast. A total of 6 of these 8 samples were included in the subset mean. Two (L and K) were excluded as they did not agree, they were also the closest to the cross-cutting dyke.

Site H1611 This site had a LN2 direction which heavily overlapped the characteristic component. This led to a sharp curve in many of the Zijderveld diagrams due to the overlapping directions. These were the only components observed. A site mean was calculated using 6 of the 8 samples, 2 were removed as they were outliers and far from the main cluster.

Site H1612 This site yielded a scattered LN2 unblocking directions and a clearer magnetite to origin component. These were the only components observed. The LN2 unblocking direction is usually in a sharply different direction from the characteristic direction, though all have positive inclinations. The characteristic direction in the samples is a clear signal beginning at 150ºC, and not showing a difference in appearance around 300ºC as other sites have. Most samples failed to show a comprehensive magnetic direction beyond 525ºC (died at 525ºC). One sample failed to lead to the origin and its component was summarized as a plane including and forced through the origin.

Site H1615 This site does not show a consistent direction across samples. Each sample shows a very clear characteristic direction (based on MTO) which is similar to its respective LN2 direction.

Site H1616 The LN2 directions are clear yet do not agree on a single direction but it yields clear characteristic directions. 7 of the 8 characteristic directions magnetite-to-origin and are equatorial northeast. The Sample D is not used in the analysis as the data do not yield a characteristic direction. Due to an overall lack of agreement, this site is not included in the analysis.

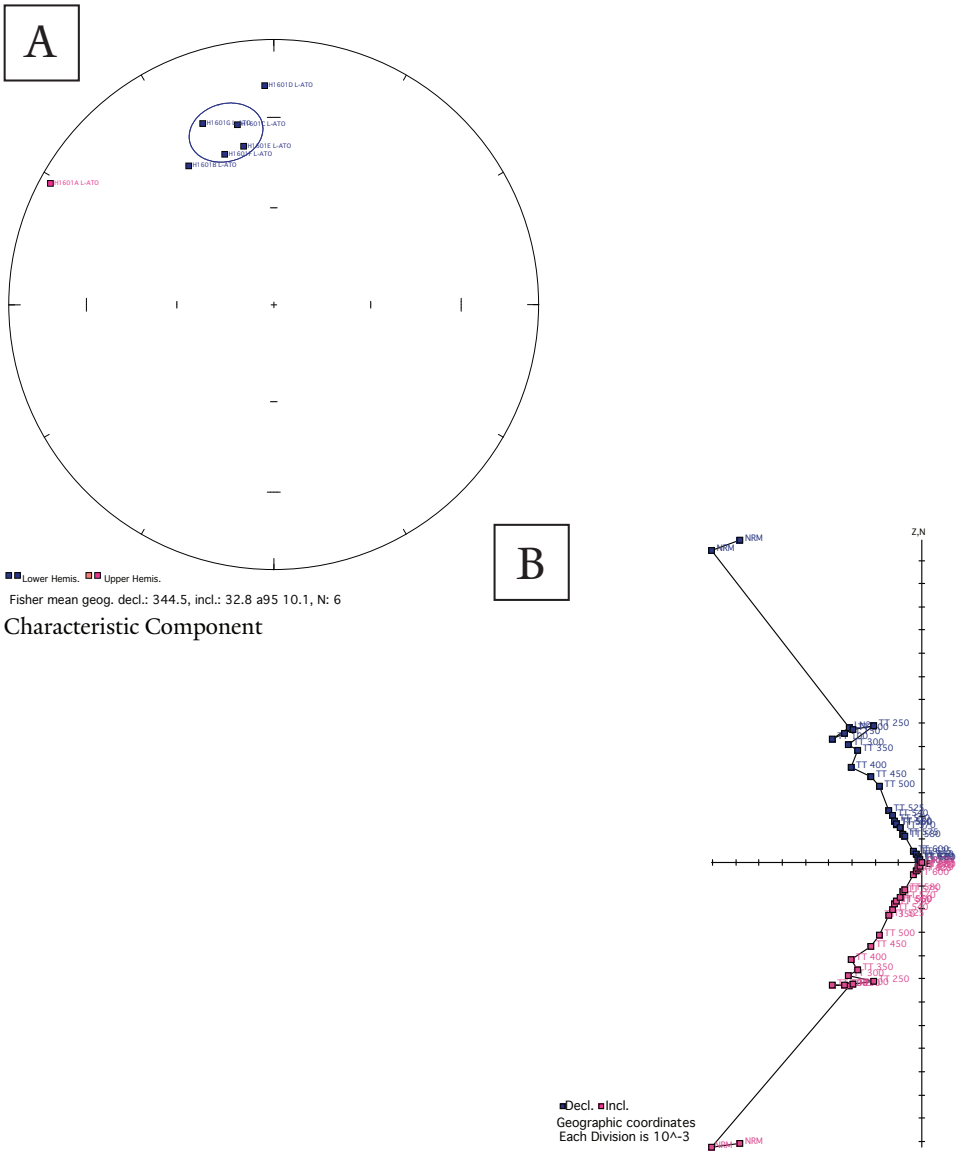

Site H1601: A. A stereonet showing the characteristic components of this site. Theses charactersitic components are ATO. Samples show a single component of magnetization, as seen in **B.** Zijerveld diagram shows H1601B, a sample which is representative of the behavior of the site.

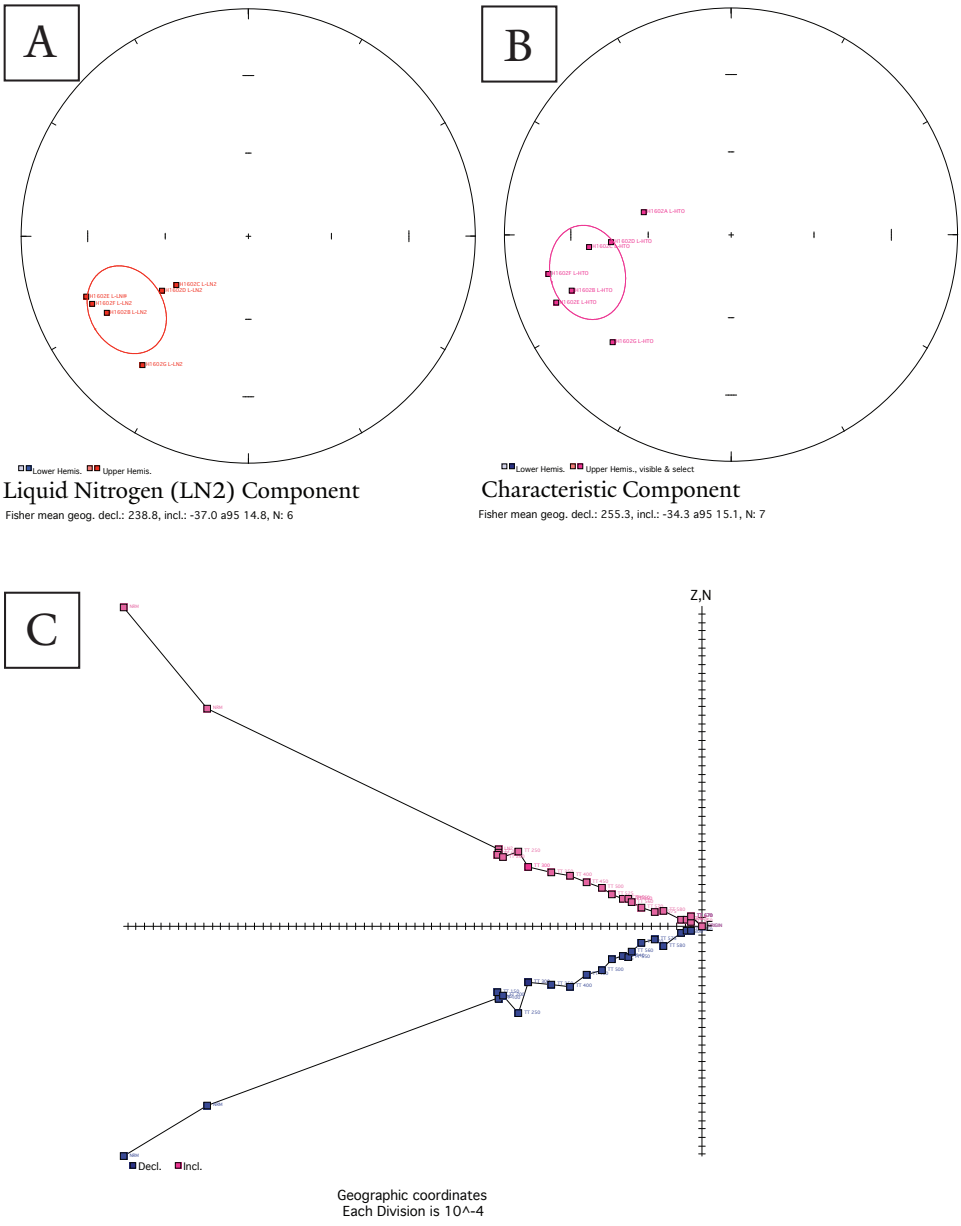

Site H1602: A & B. These stereonets show the liquid nitrogen and the characteristic components in geographic coordinates, respectively. **C.** This Zijerveld diagram shows H1602E, which is representative of the behavior of the significant samples of this site.

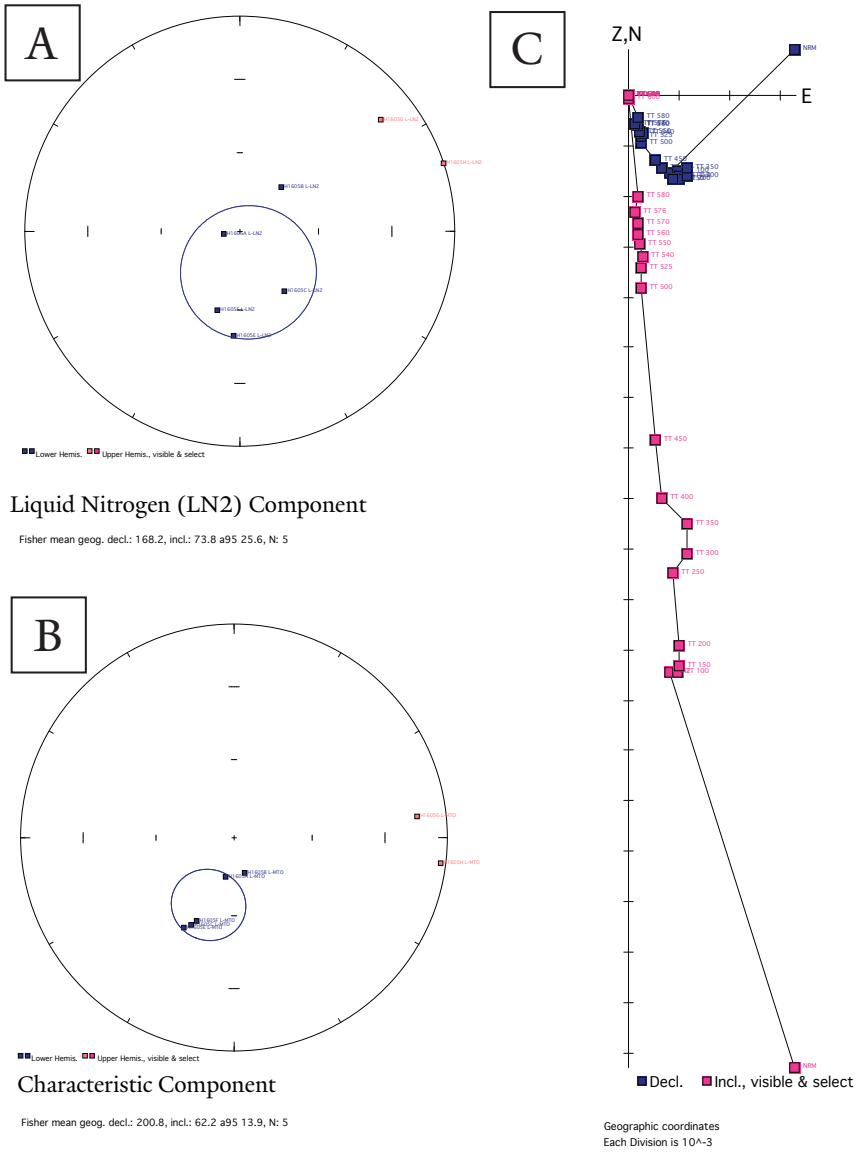

Site H1605: A & B. These stereonets show the liquid nitrogen and the characteristic components in geographic coordinates, respectively. Samples G & H are shown for completeness, but due to their distance from the mean, they are excluded from the site mean. **C.** This Zijerveld diagram shows H1605B, a sample which is representative of the behavior of the site.

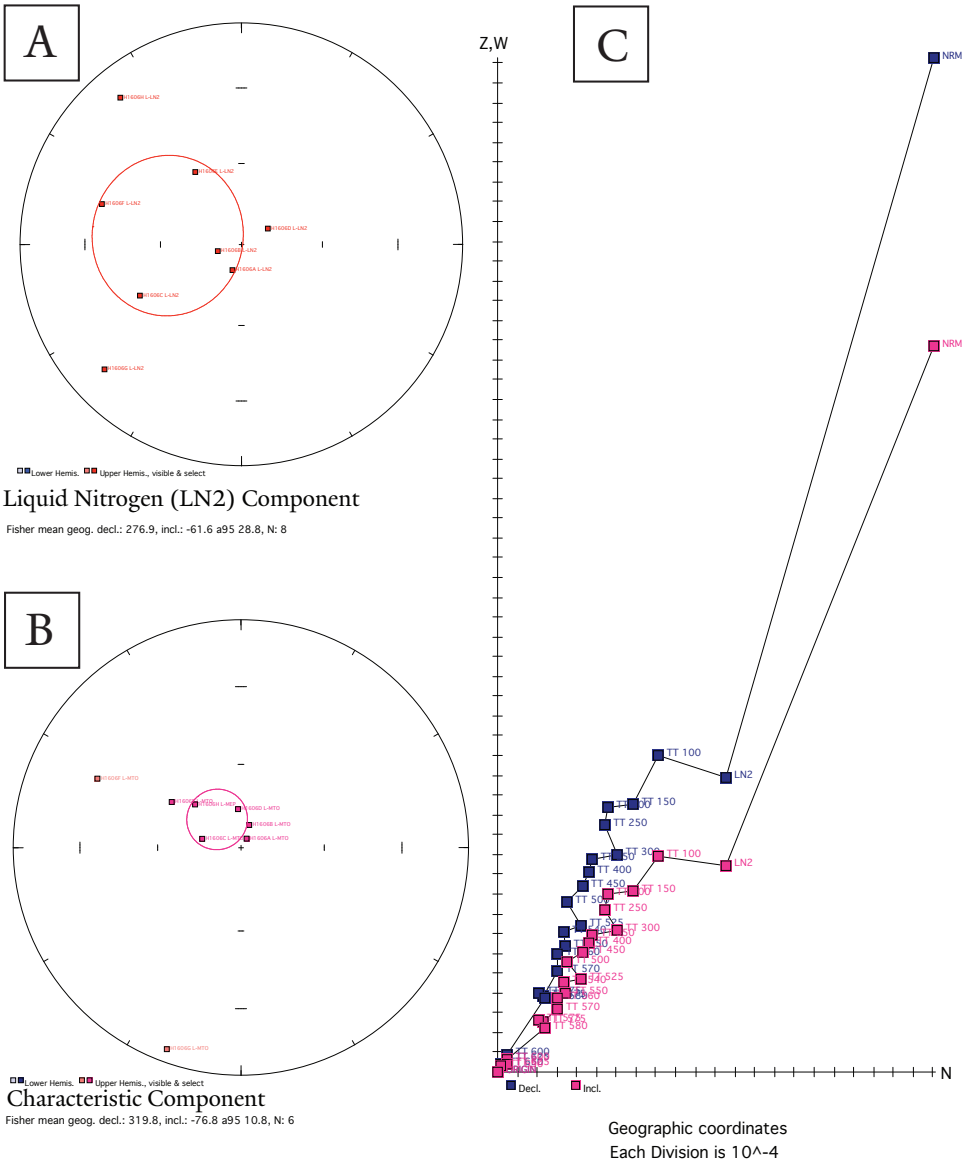

Site H1806: A & B. These stereonets show the liquid nitrogen and the characteristic components in geographic coordinates, respectively. **C.** This Zijerveld diagram shows H1806F, a sample which is representative of the behavior of the site.

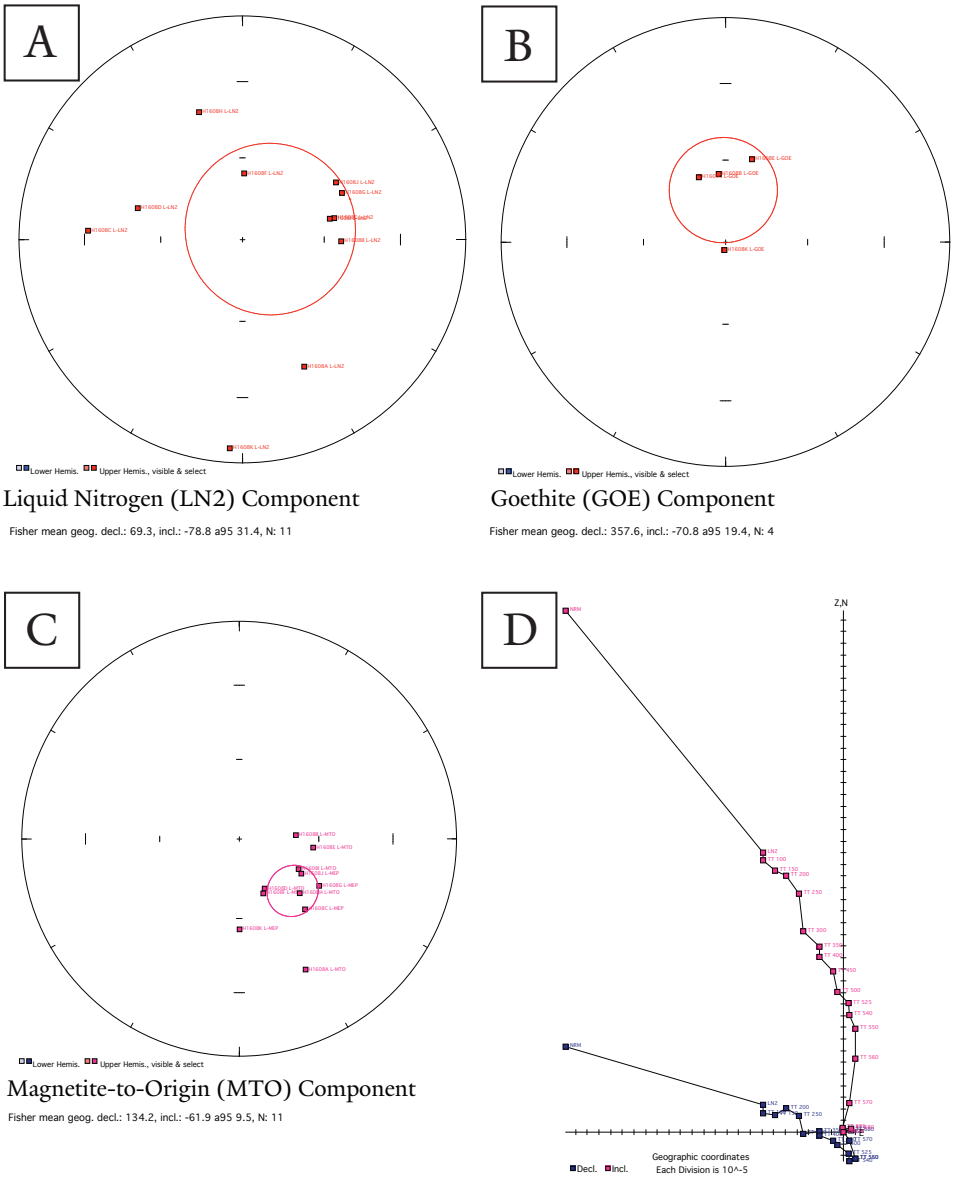

Site H1608: A-C. These stereonets show the liquid nitrogen, the goerthite, and the characteristic components in geographic coordinates, respectively. **D.** This Zijerveld diagram shows H1608D, a sample which is representative of the behavior of the site.

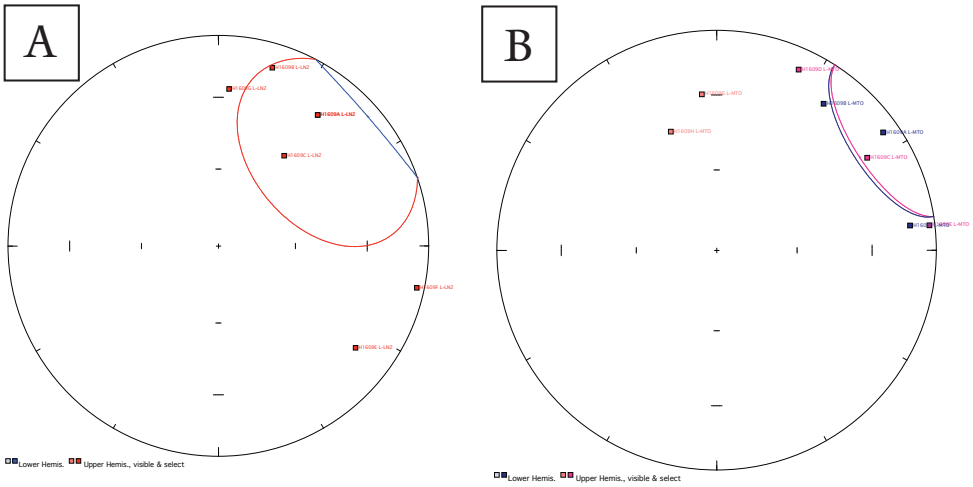

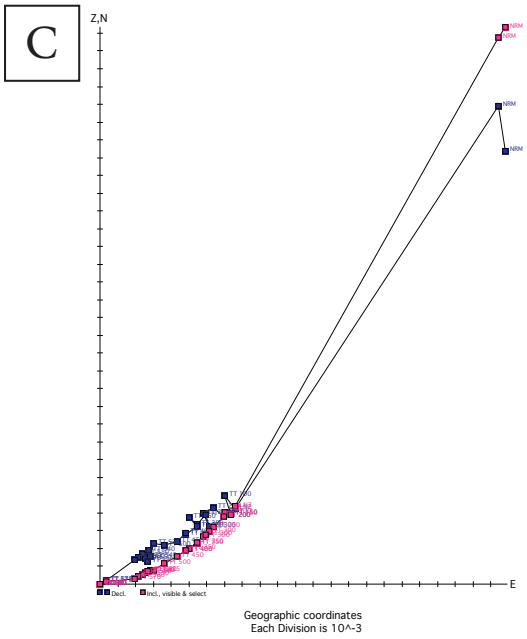

Site H1609: A & B. These stereonets show the liquid nitrogen and the characteristic components in geographic coordinates, respectively. **C.** This Zijerveld diagram shows H1609C, a sample which is representative of the behavior of the site.

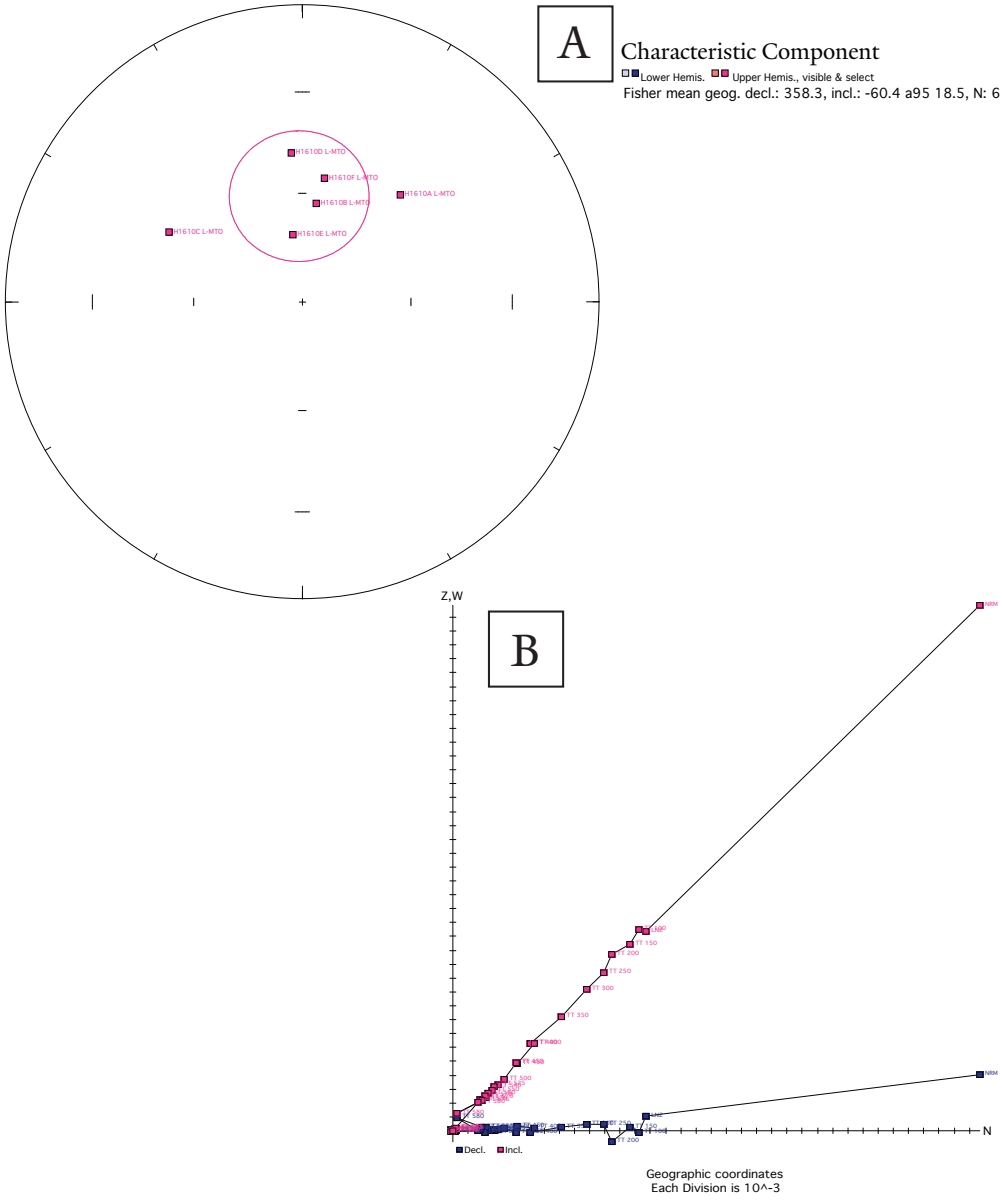

Site H1610 (Samples A-F): A. This steroenet shows characteristic component of the basement exocontact samples from this site. **B.** This Zijerveld diagram shows H1610D, a sample which is representative of the behavior of the site.

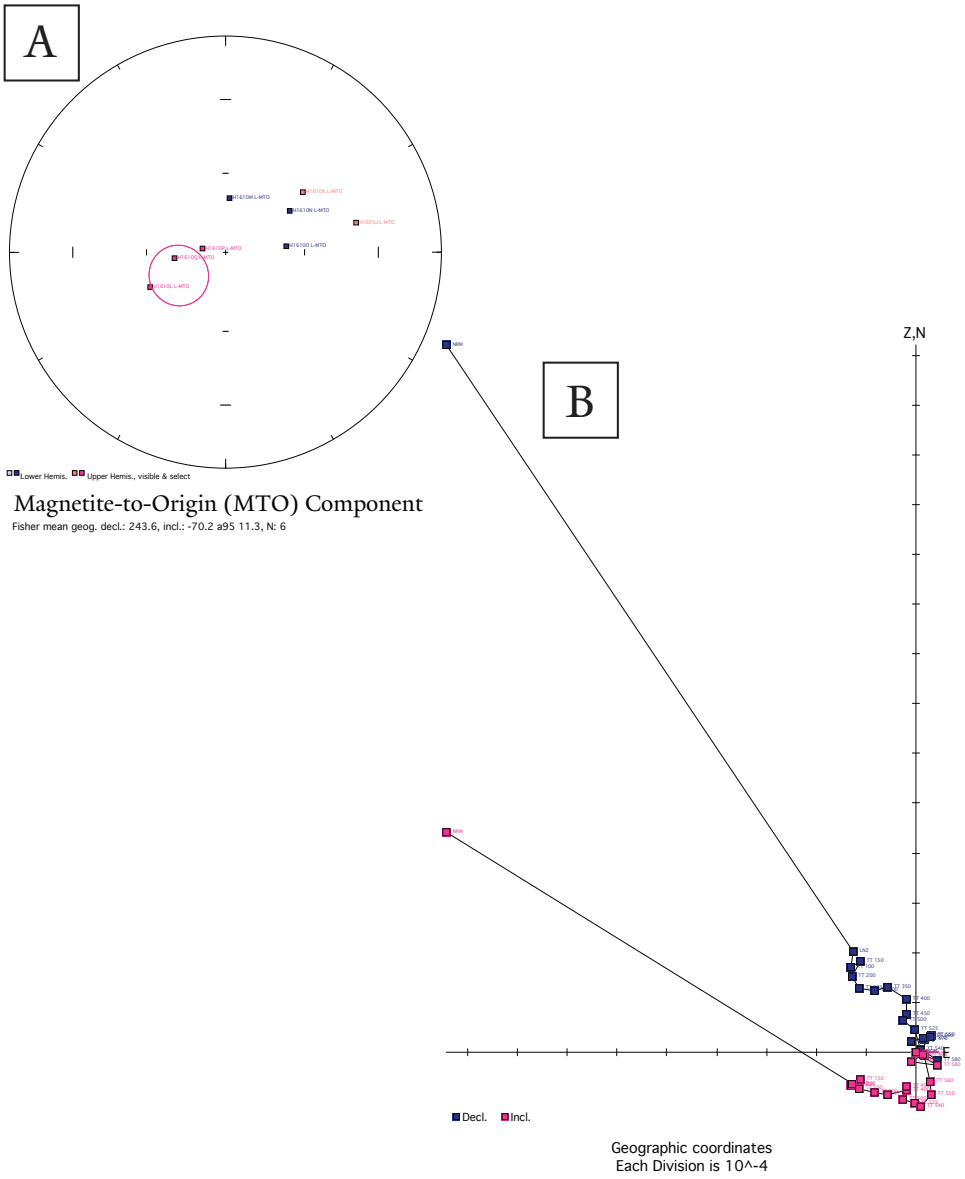

Site H1610 (Samples L-Q): A. This the characteristic components in geographic coordinates. **B.** This Zijerveld diagram shows H1610R, a sample which is representative of the behavior of the site.

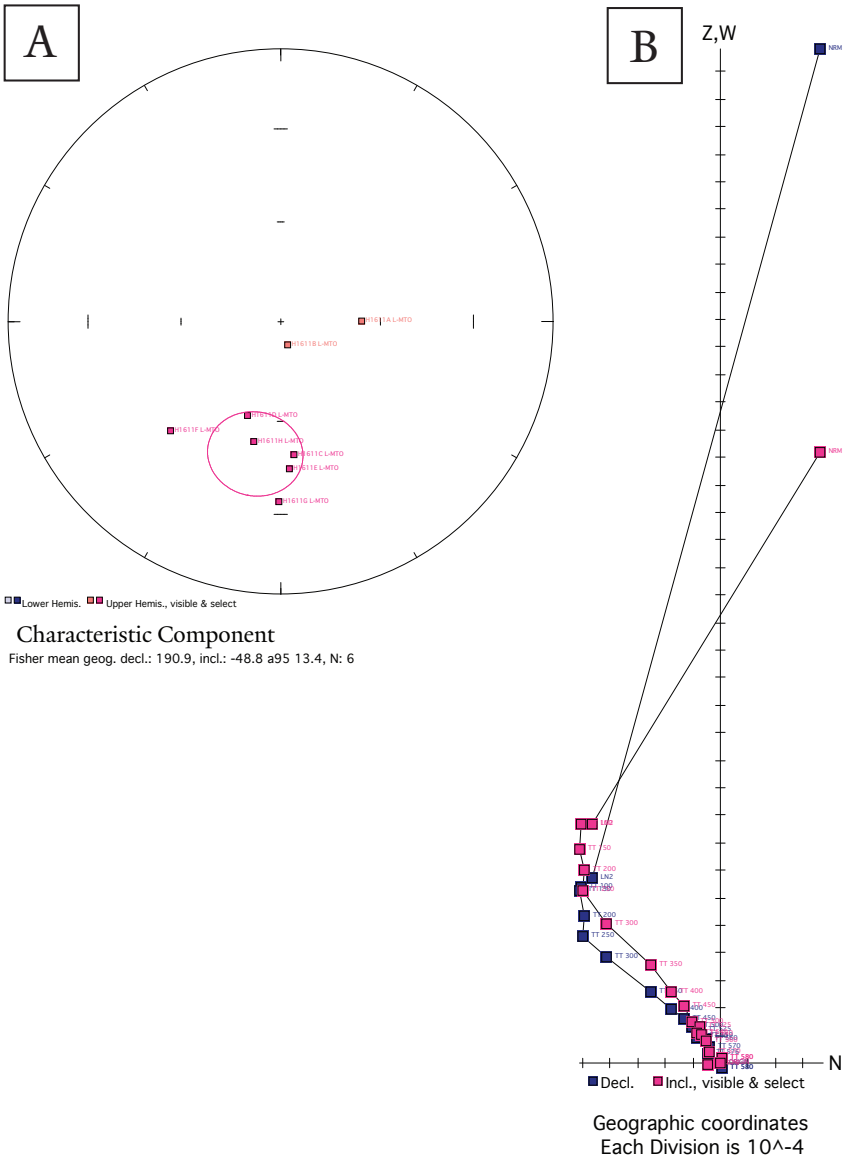

Site H1611: A. These stereonets show the characteristic components in geographic coordinates. **B.** This Zijerveld diagram shows H1611F, a sample which is representative of the behavior of the significant subset of this site.

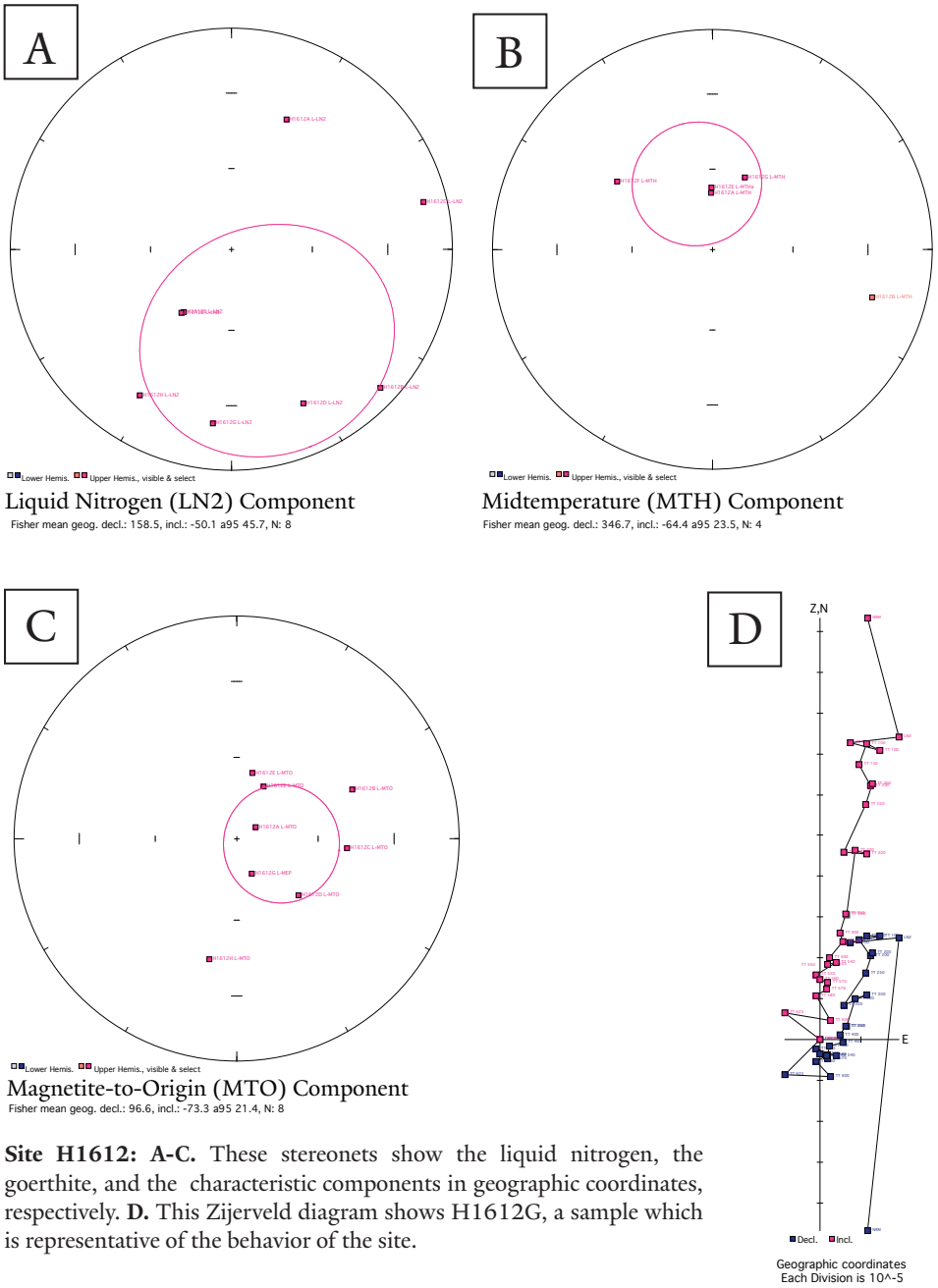

Liquid Nitrogen (LN2) Component
Fisher mean geog. decl.: 158.5, incl.: -50.1 a95 45.7, N: 8

Midtemperature (MTH) Component
Fisher mean geog. decl.: 346.7, incl.: -64.4 a95 23.5, N: 4

Magnetite-to-Origin (MTO) Component
Fisher mean geog. decl.: 96.6, incl.: -73.3 a95 21.4, N: 8

Geographic coordinates
Each Division is 10^-5

Site H1612: A-C. These stereonets show the liquid nitrogen, the goerthite, and the characteristic components in geographic coordinates, respectively. **D.** This Zijerveld diagram shows H1612G, a sample which is representative of the behavior of the site.

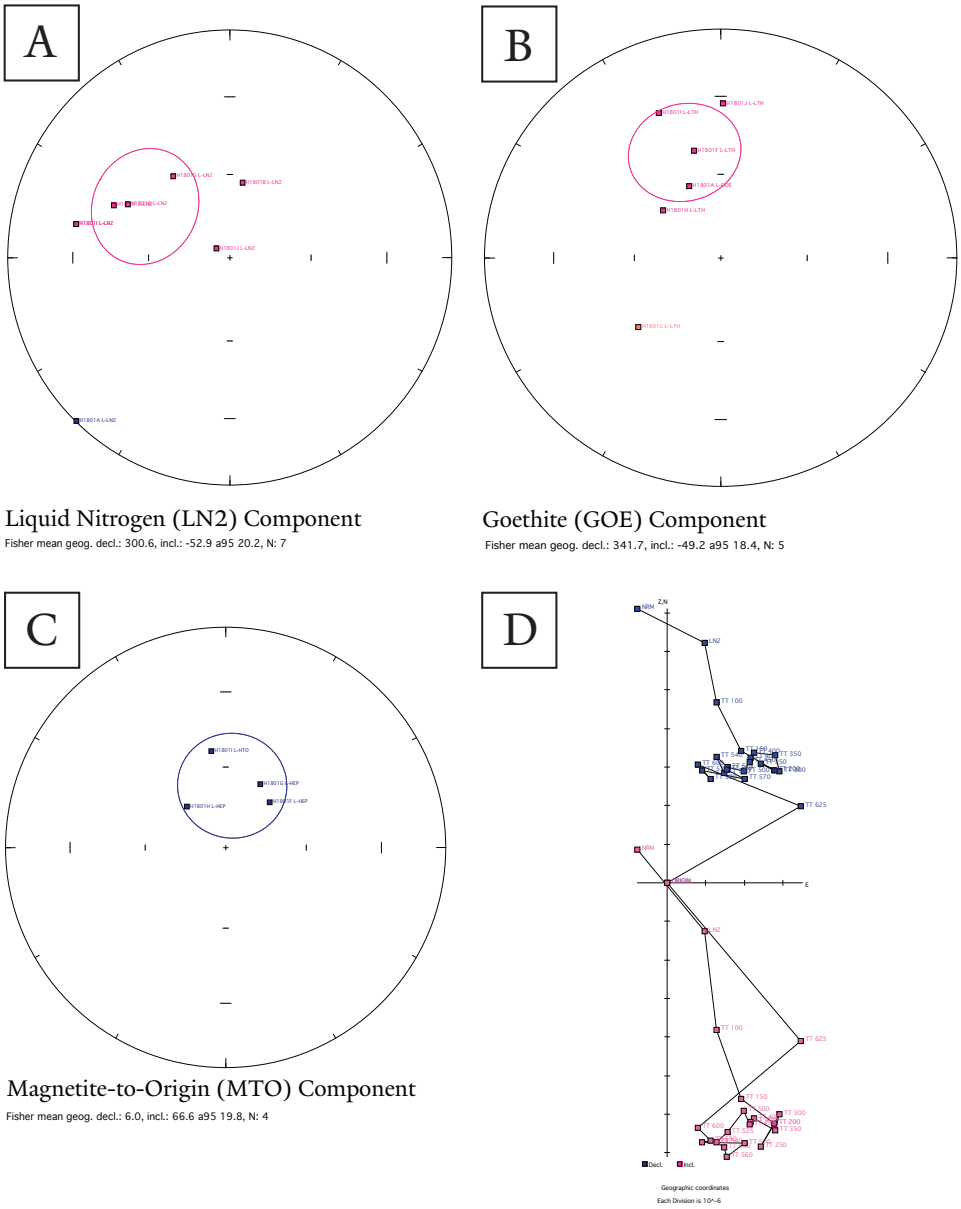

Site H1801: A-C. These stereonets show the liquid nitrogen, the goerthite, and the characteristic components in geographic coordinates, respectively. **D.** This Zijerveld diagram shows H1801G, a sample which is representative of the behavior of the site.

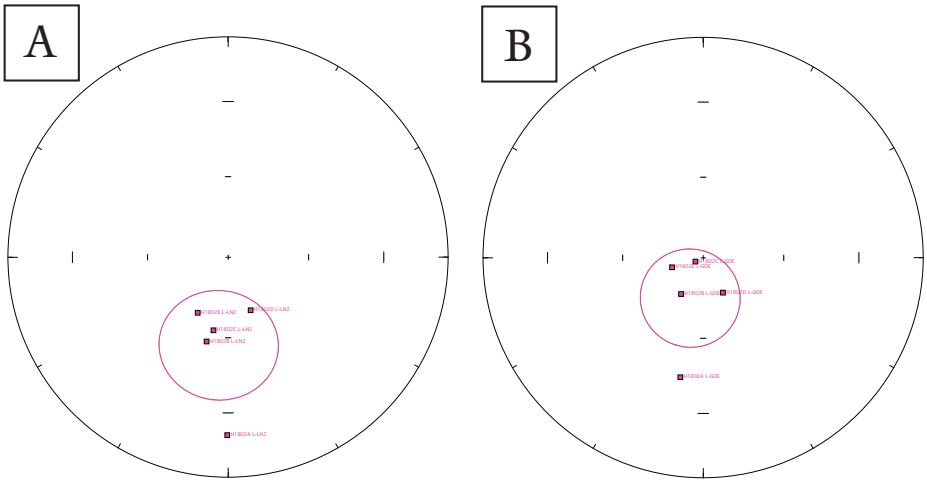

Liquid Nitrogen (LN2) Component

Fisher mean geog. decl.: 186.1, incl.: -56.4 a95 21.2, N: 5

Goethite (GOE) Component

Fisher mean geog. decl.: 197.8, incl.: -74.1 a95 18.3, N: 5

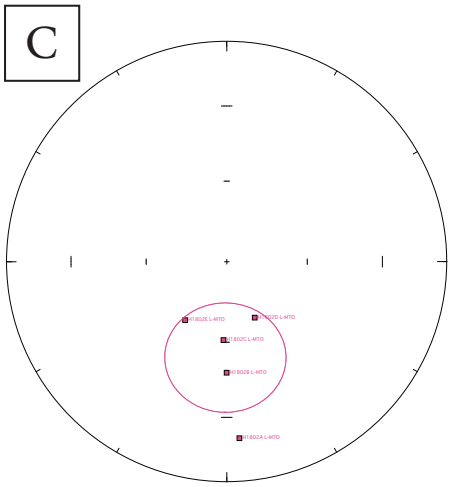

Magnetite-to-Origin (MTO) Component

Fisher mean geog. decl.: 180.8, incl.: -53.4 a95 21.3, N: 5

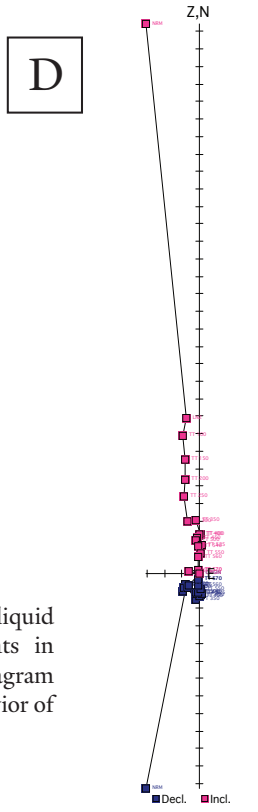

Geographic coordinates
Each Division is 10^-6

Site H1802 (Samples A-E): A-C. These stereonets show the liquid nitrogen, the goerthite, and the characteristic components in geographic coordinates, respectively. **D.** This Zijerveld diagram shows H1802C, a sample which is representative of the behavior of the site.

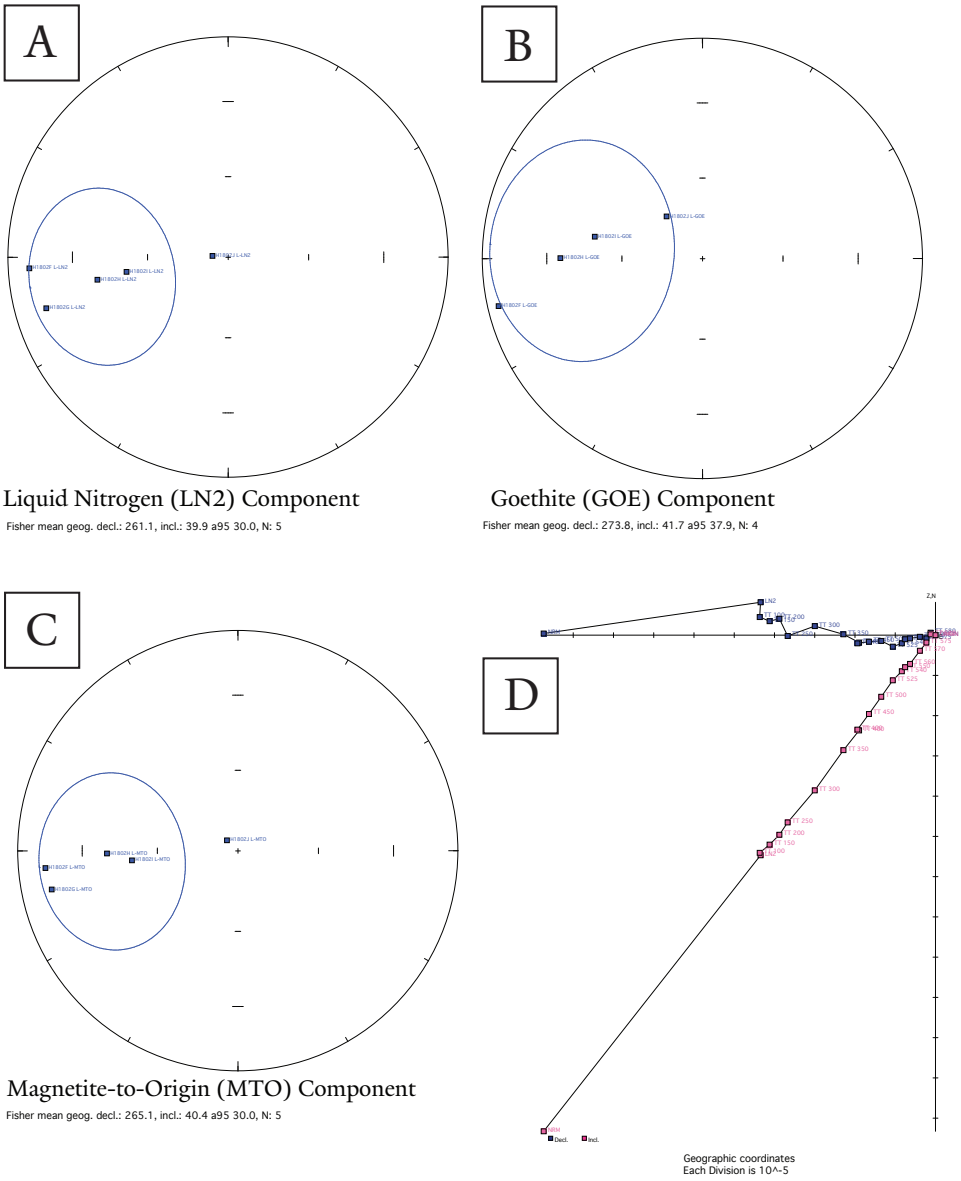

Site H1802 (F-J): A-C. These stereonets show the liquid nitrogen, the goerthite, and the characteristic components in geographic coordinates, respectively. **D.** This Zijerveld diagram shows H1802I, a sample which is representative of the behavior of this subset of the site.

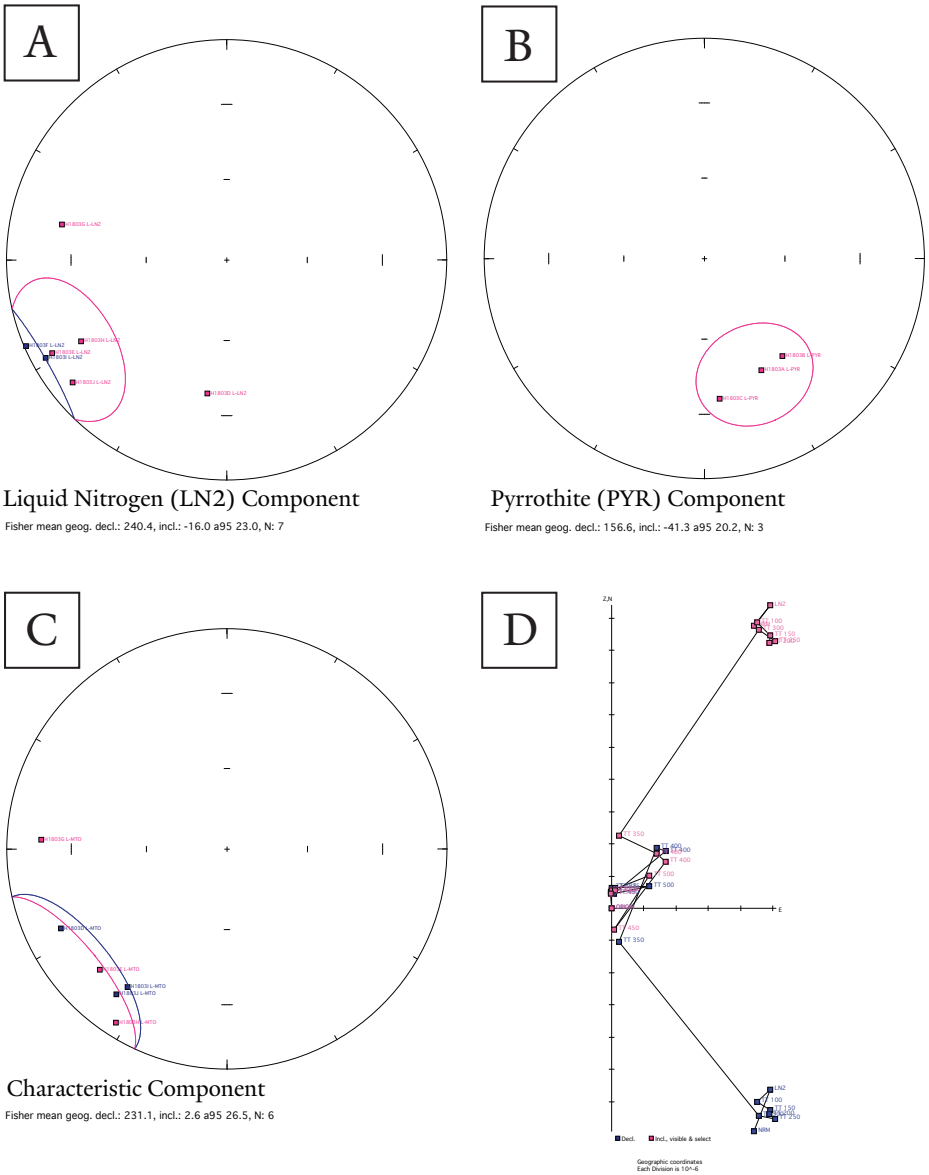

Site H1803: A-C. These stereonets show the liquid nitrogen, the pyrrothite, and the characteristic components in geographic coordinates, respectively. **D.** This Zijerveld diagram shows H1803B, a sample which is representative of the behavior of the site.

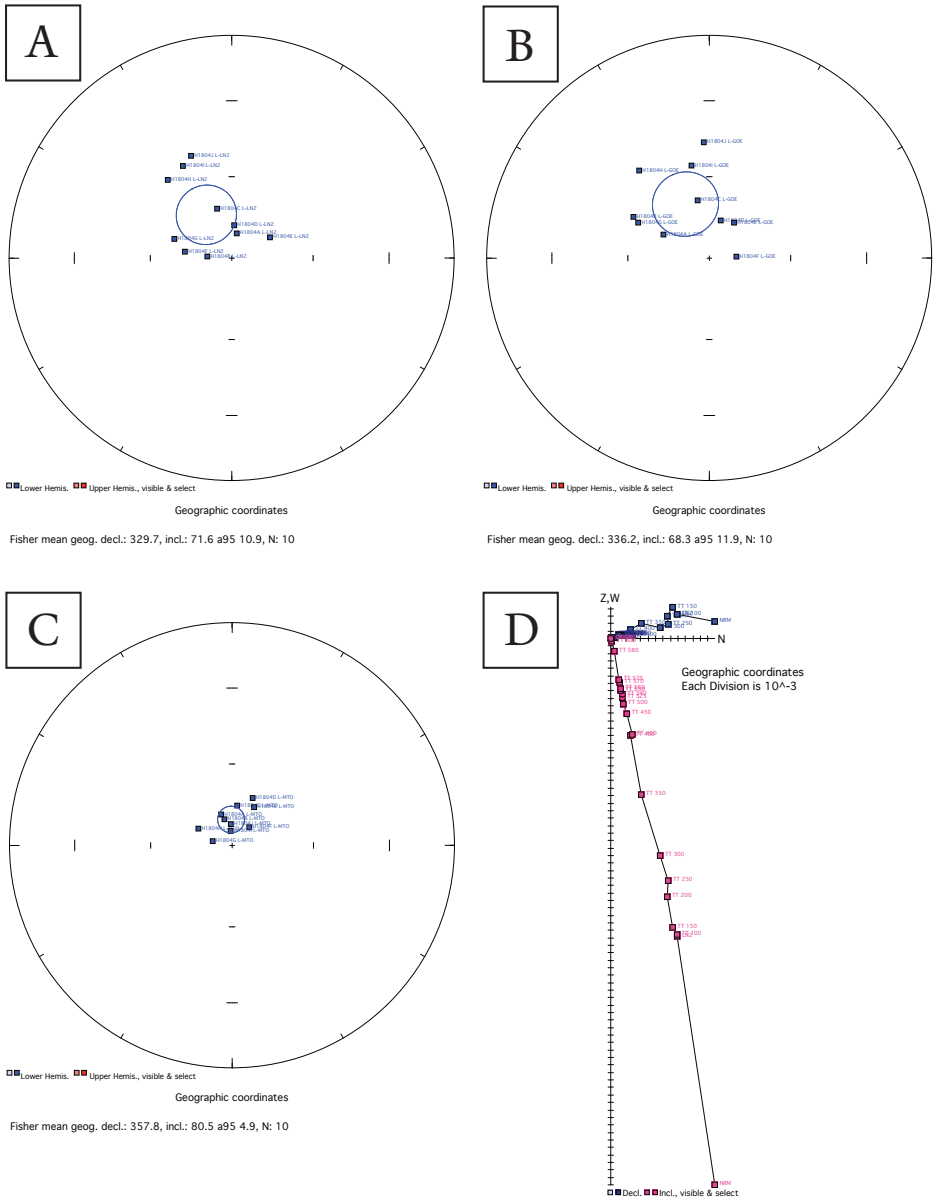

Site H1804: A-C. These stereonets show the liquid nitrogen, the goerthite, and the characteristic components, respectively. **D.** This Zijerveld diagram shows H1804A, a sample which is representative of the behavior of the site.

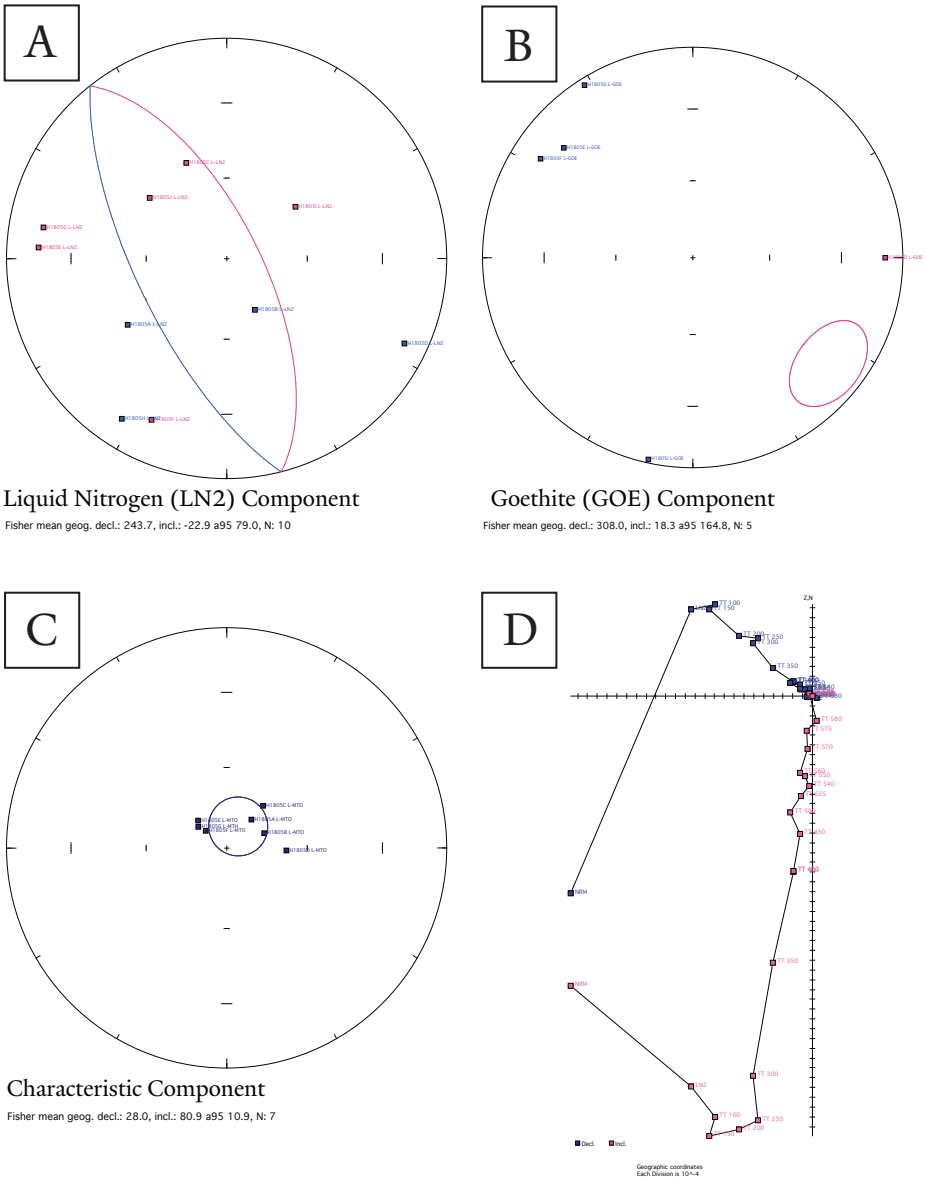

Site H1805: A-C. These stereonets show the liquid nitrogen, the goerthite, and the characteristic components in geographic coordinates, respectively. **D.** This Zijerveld diagram shows H1805F, a sample which is representative of the behavior of the site.

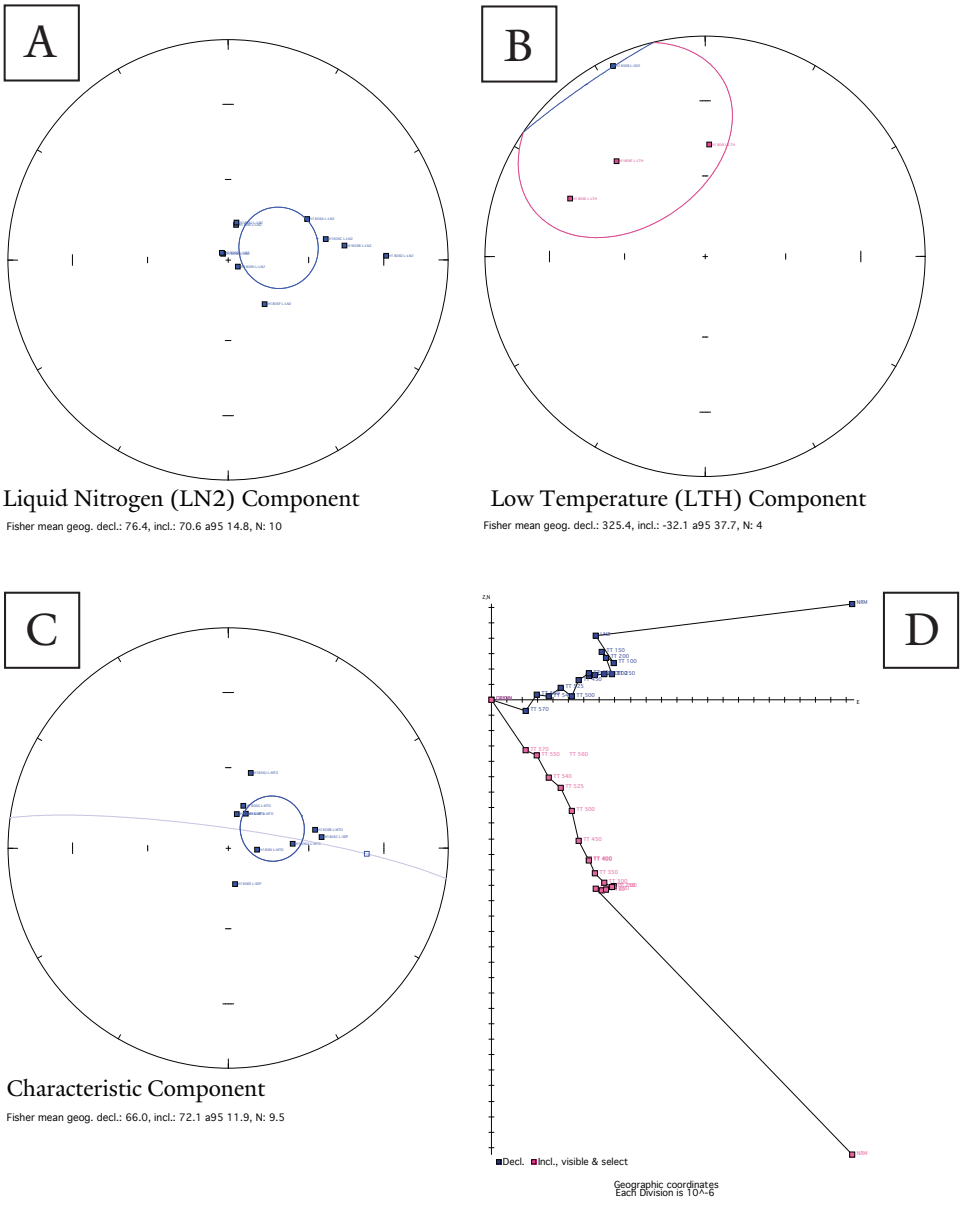

Site H1806: A-C. These stereonets show the liquid nitrogen, the low temperature, and the characteristic components in geographic coordinates, respectively. **D.** This Zijerveld diagram shows H1806B, a sample which is representative of the behavior of the site.

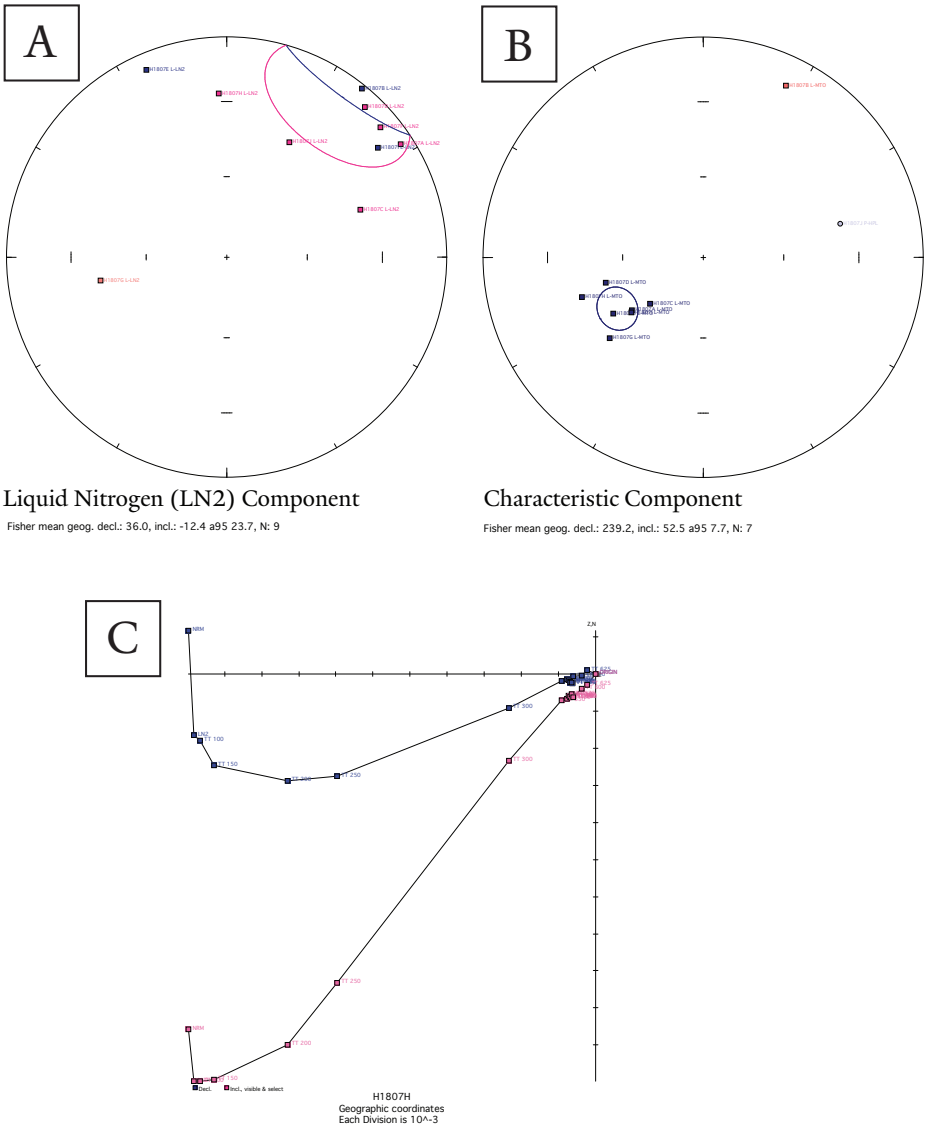

Site H1807: A. This stereonet shows the liquid nitrogen component observed in demagnetization. **B.** This stereonet shows the characteristic components of the demagnetization. **C.** This Zijerveld diagram shows H1807H, a sample which is representative of the behavior of the site.

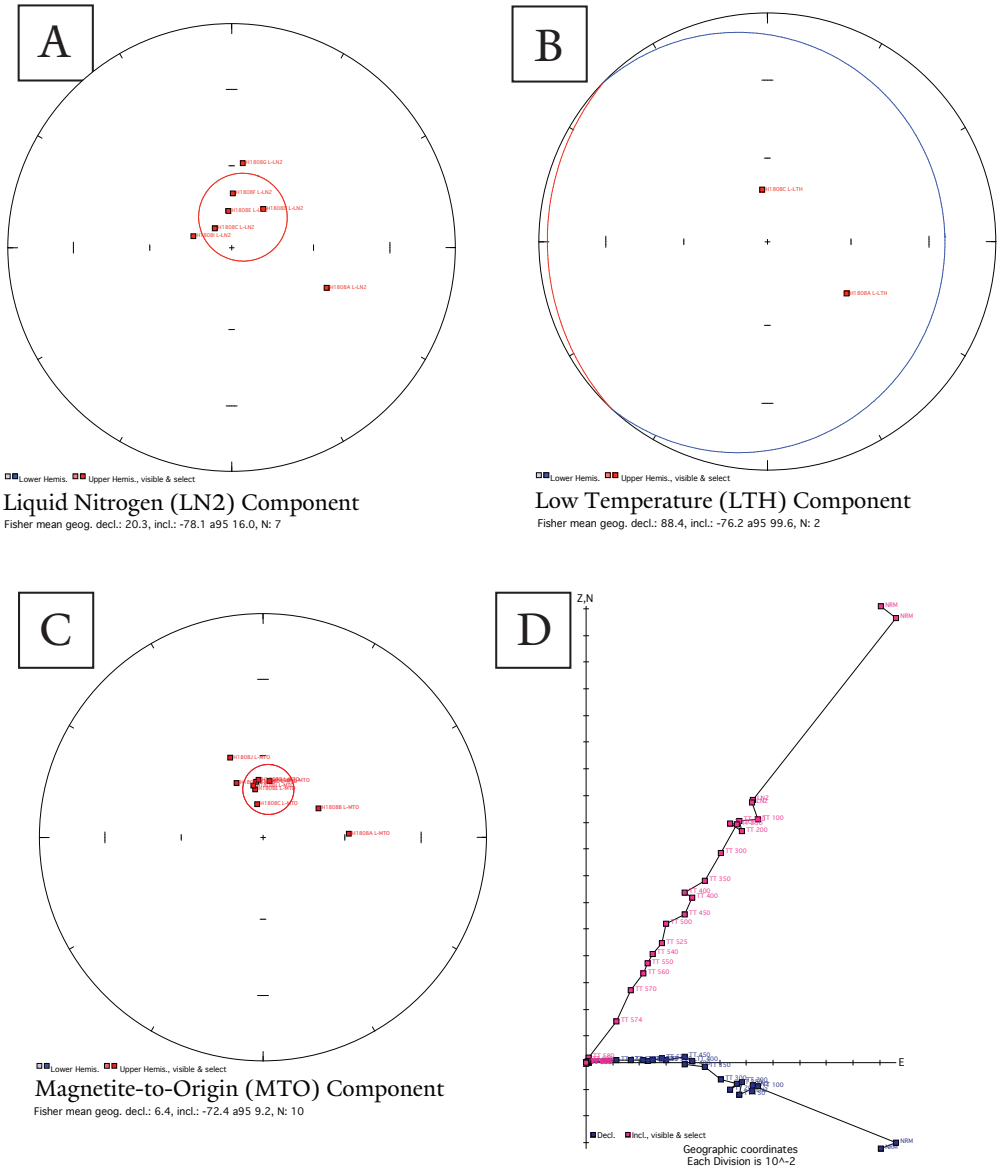

Site H1808: A-C. These stereonets show the liquid nitrogen, the low temperature, and the characteristic components in geographic coordinates, respectively. **D.** This Zijerveld diagram shows H1808A, a sample which is representative of the behavior of the site.

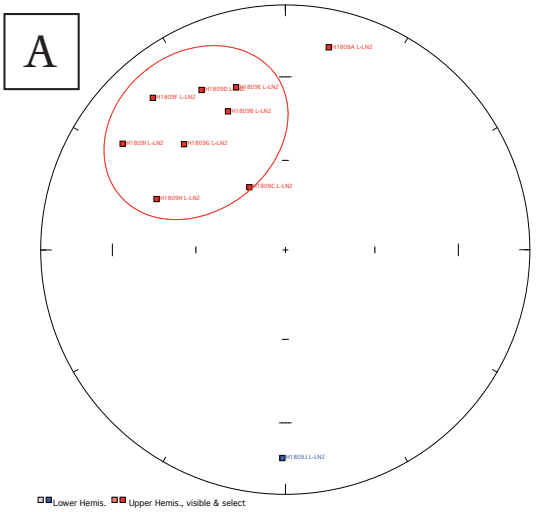

Liquid Nitrogen (LN2) Component
Fisher mean geog. decl.: 322.6, incl.: -37.4 a95 29.6, N: 10

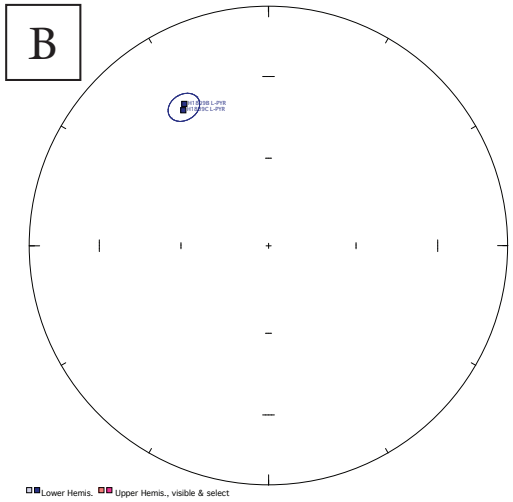

Phyrrotite (PYR) Component
Fisher mean geog. decl.: 328.6, incl.: 32.7 a95 5.0, N: 2

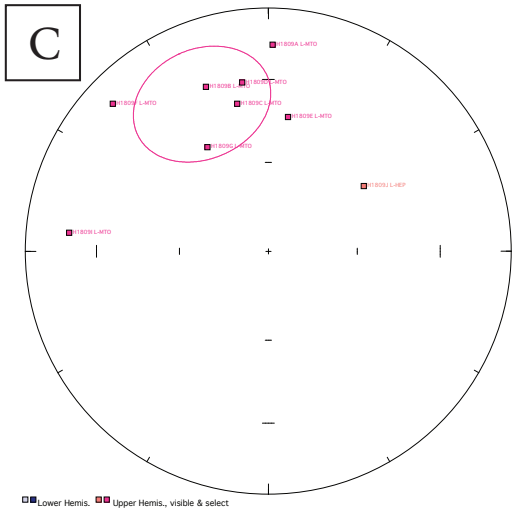

Characteristic Component
Fisher mean geog. decl.: 335.7, incl.: -32.8 a95 21.0, N: 8

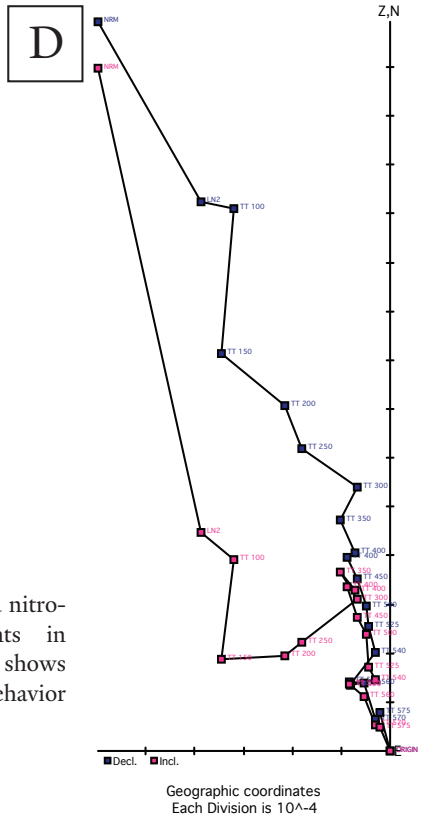

Geographic coordinates
Each Division is 10^-4

Site H1809: A-C. These stereonets show the liquid nitrogen, phyrrotite, and characteristic components in geographic coordinates. **D.** This Zijerveld diagram shows H1809C, a sample which is representative of the behavior of the site.

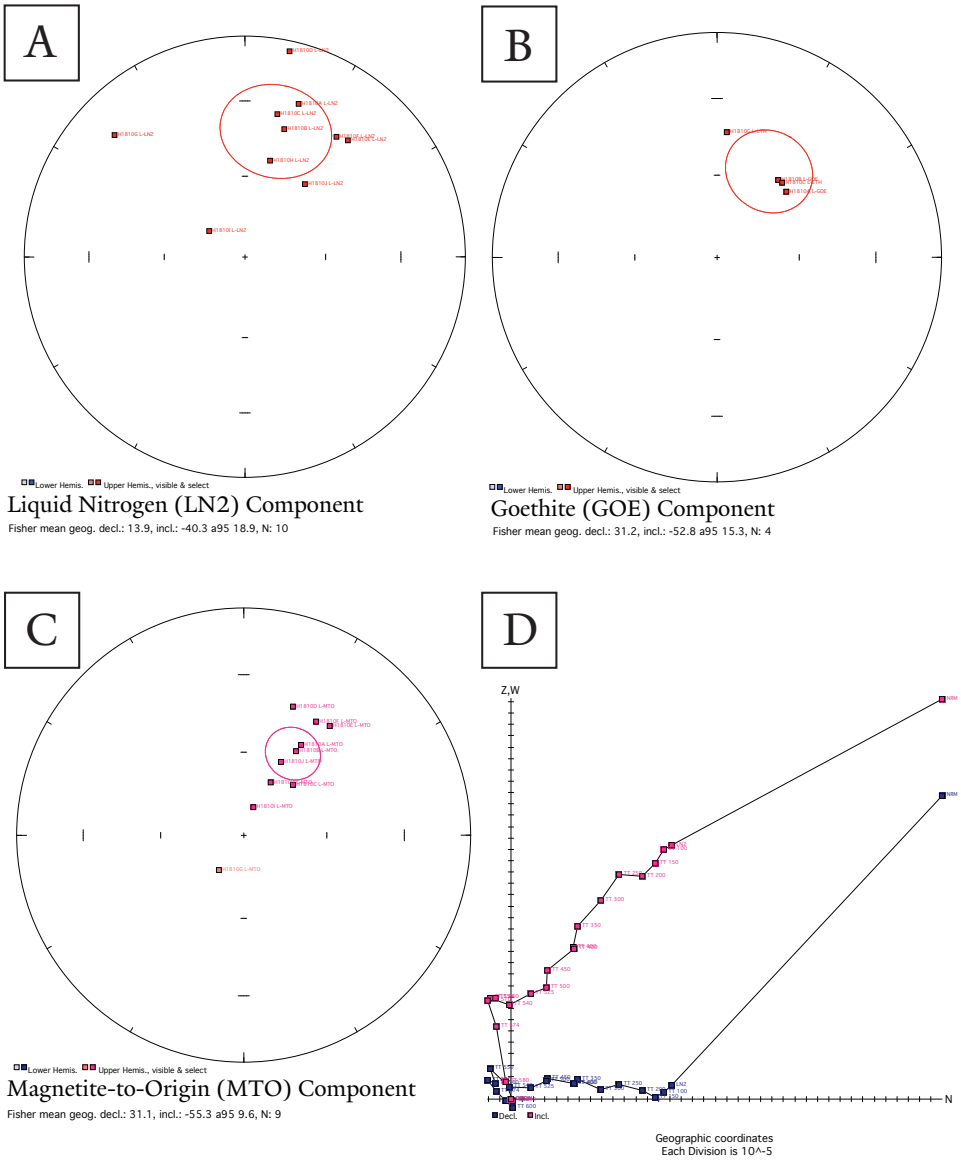

Site H1810: A-C. These stereonets show the liquid nitrogen, the goerthite, and the characteristic components in geographic coordinates, respectively. **D.** This Zijerveld diagram shows H1810G, a sample which is representative of the behavior of the site.

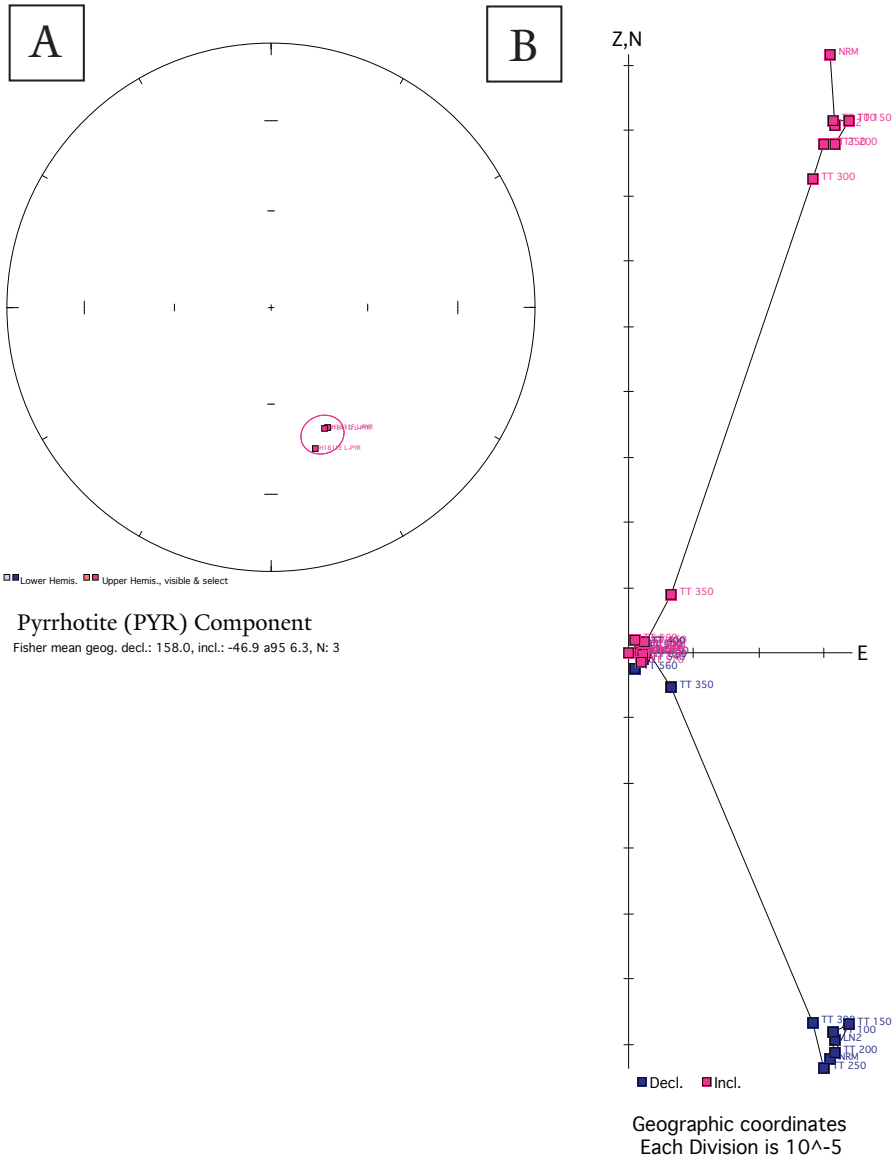

Site H1811: A. These stereonets show the pyrrhotite components in geographic coordinates, respectively. **B.** This Zijerveld diagram shows H1811G, a sample which is representative of the behavior of the site. The large demagnetization step between 300 and 350ºC supports a pyrrhotite component.

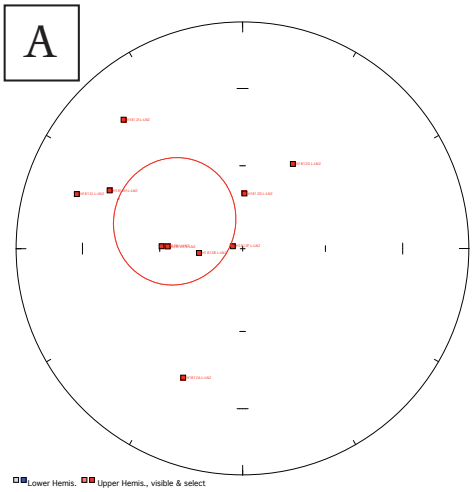

Liquid Nitrogen (LN2) Component

Fisher mean geog. decl.: 291.9, incl.: -63.1 a95 22.5, N: 10

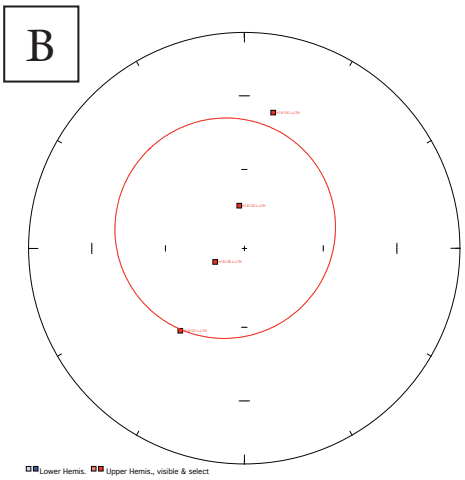

Low Temperature (LTH) Component

Fisher mean geog. decl.: 316.5, incl.: -78.8 a95 42.4, N: 4

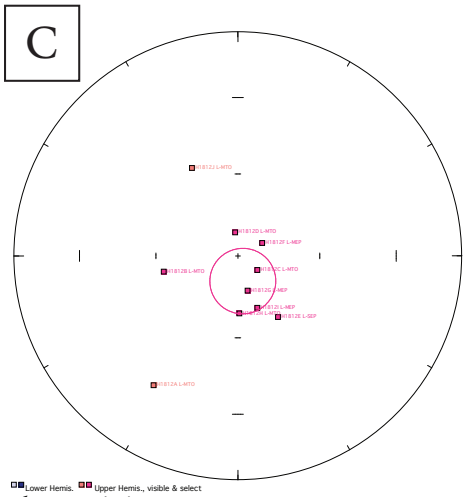

Characteristic Component

Fisher mean geog. decl.: 168.9, incl.: -80.6 a95 11.9, N: 8

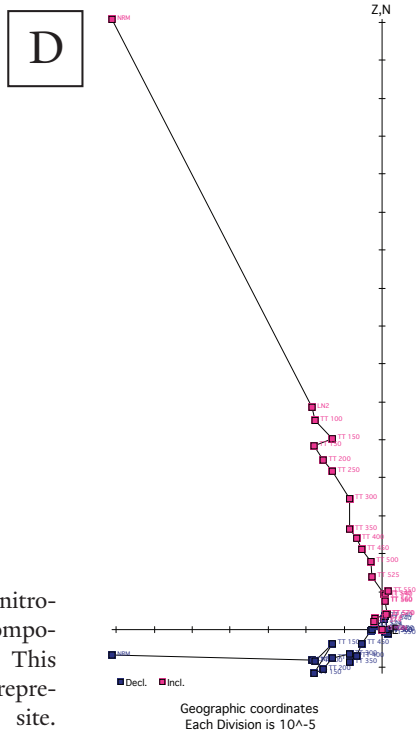

Site H1812: A-C. These stereonets show the liquid nitrogen, the low temperature, and the characteristic components in geographic coordinates, respectively. **D.** This Zijerveld diagram shows H1812C, a sample which is representative of the behavior of the site.

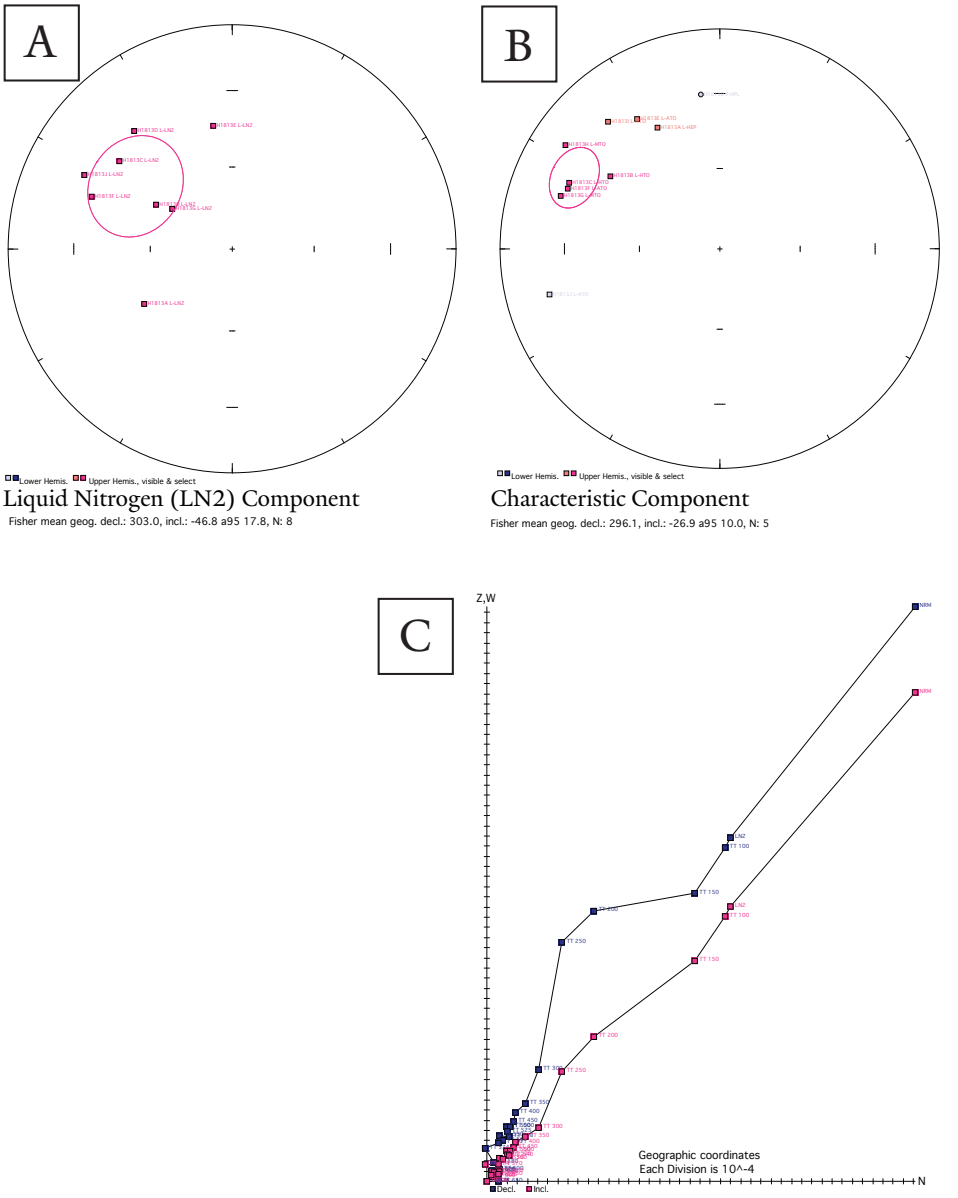

Site H1813: A & B. These stereonets show the liquid nitrogen and the characteristic components in geographic coordinates, respectively. **C.** This Zijerveld diagram shows H1813C, a sample which is representative of the behavior of the site.

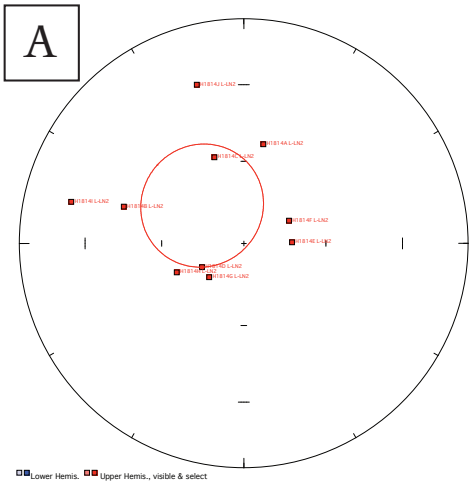

Liquid Nitrogen (LN2) Component

Fisher mean geog. decl.: 312.2, incl.: -69.2 a95 22.3, N: 10

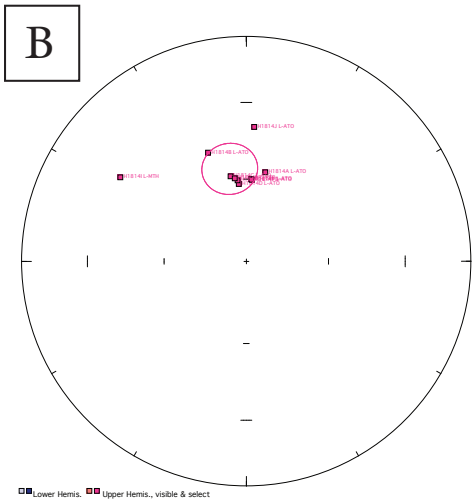

Characteristic Component

Fisher mean geog. decl.: 349.8, incl.: -55.5 a95 9.6, N: 10

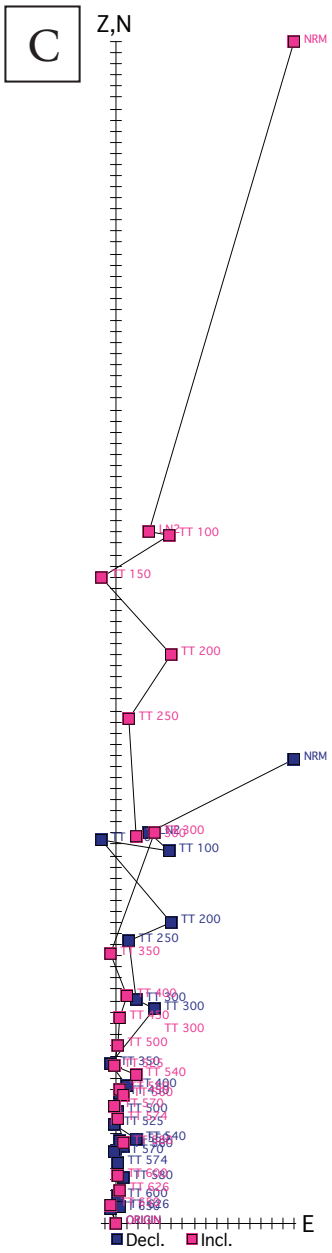

Geographic coordinates
Each Division is 10^-4

Site H1814: A & B. These stereonets show the liquid nitrogen and the characteristic components in geographic coordinates. **C.** This Zijerveld diagram shows H1814F, a sample which is representative of the behavior of the site.

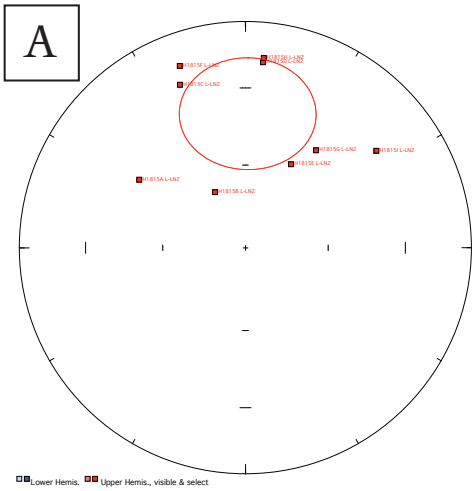

Liquid Nitrogen (LN2) Component

Fisher mean geog. decl.: 0.9, incl.: -39.4 a95 22.3, N: 9

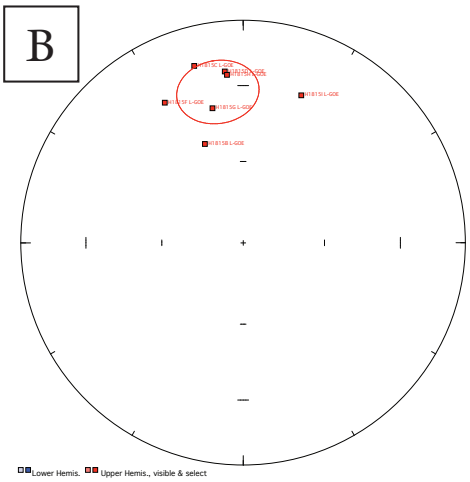

Goethite (GOE) Component

Fisher mean geog. decl.: 350.5, incl.: -31.4 a95 13.2, N: 7

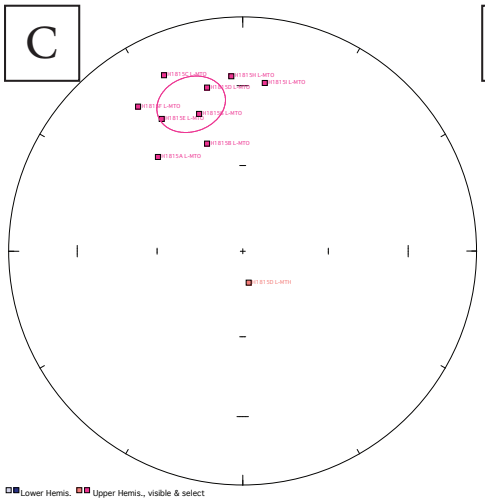

Magnetite-to-Origin (MTO) Component

Fisher mean geog. decl.: 340.6, incl.: -33.6 a95 10.7, N: 9

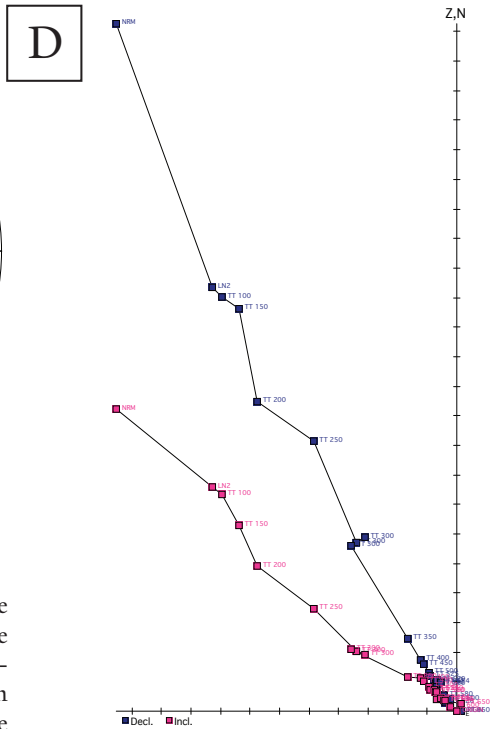

Site H1815: A-C. These stereonets show the liquid nitrogen, the goerthite, and the characteristic components in geographic coordinates, respectively. **D.** This Zijerveld diagram shows H1815F, a sample which is representative of the behavior of the site.

David Evans, 10/23/10

Program to give the mean of vectors in D,I coordinates — 1 =incl flattening factor — 0.0175 =PI/180

New: 2-polarity change to 1 in columns H,I; adjust formulas as necessary to split data

Site	Decl	Incl	a-95 °	weight	n		Chosen polarity Decl	Chosen polarity Incl	f(I)	D,I(radians)		N	E	U	Site location Lat °N	Site location Long °E	° Paleolat	Butler, p.301 Butler's ß	Butler, p.301 ambig. test	Pole location Lat °N	Pole location Long °E	(in radians)		North	Greenw.	NinetyE
ChRMs: MTO							000.0	00.0	00.0	0	0	0	0	0			00.0	#DIV/0!	0.000	90.0	#DIV/0!	1.571	#DIV/0!			
H1801 (F-I) hematite	006.0	66.6	19.6	0	4	10	006.0	66.6	66.6	0.105	1.162	0	0	0	-20.4	014.9	49.1	4.18	0.877	20.3	019.0	0.355	0.332			
H1802 (A-E)	180.8	-53.4	21.3	0	5	10	000.8	53.4	53.4	0.014	0.932	0	0	0	-20.4	014.9	34.0	0.82	0.761	35.7	015.7	0.623	0.274			
H1802 (F-J)	265.1	40.4	30.0	0	5	10	265.1	40.4	40.4	4.627	0.705	0	0	0	-20.4	014.9	23.1	-69.66	0.319	-12.1	-054.8	-0.211	-0.957			
H1803 (A-C) po	156.6	-41.3	20.2	0	3	10	336.6	41.3	41.3	5.875	0.721	0	0	0	-20.4	014.9	23.7	-28.52	0.628	40.4	-013.7	0.705	-0.238			
H1803 (D-J) same as LN2	231.1	02.6	26.5	0	6	10	231.1	02.6	02.6	4.033	0.045	0	0	0	-20.4	014.9	01.3	-75.79	-0.185	-36.6	270.6	-0.639	4.724			
H1804	357.8	80.5	4.9	1	10	10	357.8	80.5	80.5	6.245	1.405	0.1649	-0.01	-0.99	-20.4	014.9	71.5	-0.70	0.937	-01.9	014.2	-0.032	0.247	-0.032	0.969	0.2445
H1805	028.0	80.9	10.9	1	7	10	028.0	80.9	80.9	0.489	1.412	0.1396	0.074	-0.99	-20.4	014.9	72.2	8.26	0.925	-04.5	023.1	-0.079	0.404	-0.079	0.917	0.3914
H1806 young	061.8	73.7	11.1	1	9	10	061.8	73.7	73.7	1.079	1.286	0.1326	0.247	-0.96	-20.4	014.9	59.7	26.50	0.837	-04.4	041.4	-0.077	0.722	-0.077	0.748	0.6589
H1807 exocontact	239.2	52.5	7.7	0	7	10	239.2	52.5	52.5	4.175	0.916	0	0	0	-20.4	014.9	33.1	-63.25	0.340	-36.3	-048.4	-0.634	-0.845			
H1808 old	006.4	-72.4	9.2	1	10	10	186.4	72.4	72.4	3.253	1.264	-0.3	-0.03	-0.95	-20.4	014.9	57.6	-5.62	0.569	-52.4	009.2	-0.915	0.161	-0.793	0.602	0.0978
H1809	335.7	-32.8	21.0	0	8	10	155.7	32.8	32.8	2.717	0.572	0	0	0	-20.4	014.9	17.9	87.94	-0.013	-66.9	106.9	-1.168	1.866			
H1810 MTO mode	031.1	-55.3	9.6	0	9	10	211.1	55.3	55.3	3.684	0.965	0	0	0	-20.4	014.9	35.8	-53.71	0.288	-58.7	-038.9	-1.025	-0.678			
H1810 (G) MTO	215.4	-74.7	MAD 3.1	0	1	10	035.4	74.7	74.7	0.618	1.304	0	0	0	-20.4	014.9	61.3	16.18	0.899	03.5	031.0	0.062	0.542			
H1811 (E-G) pyrrhotite	158.0	-46.9	6.3	0	3	11	338.0	46.9	46.9	5.899	0.819	0	0	0	-20.4	014.9	28.1	-24.46	0.681	37.1	-009.6	0.647	-0.168			
H1812 Tunbl~540	168.9	-80.6	11.9	1	8	10	348.9	80.6	80.6	6.089	1.407	0.1603	-0.03	-0.99	-20.4	014.9	71.7	-3.47	0.935	-02.3	011.4	-0.041	0.199	-0.041	0.979	0.1973
H1813	296.1	-26.9	10.0	0	5	10	116.1	26.9	26.9	2.026	0.469	0	0	0	-20.4	014.9	14.2	84.60	0.077	-29.0	099.5	-0.507	1.736			
H1814 ATO mode	356.9	-56.4	5.9	0	9	10	176.9	56.4	56.4	3.087	0.984	0	0	0	-20.4	014.9	37.0	8.58	0.268	-73.2	023.4	-1.277	0.409			
H1814 (I) MTH	303.7	-33.1	MAD 6.2	0	1	10	123.7	33.1	33.1	2.159	0.578	0	0	0	-20.4	014.9	18.1	82.29	0.100	-37.0	097.1	-0.646	1.696			
H1815 MTO	340.6	-33.6	10.7	0	9	9	160.6	33.6	33.6	2.803	0.586	0	0	0	-20.4	014.9	18.4	87.15	-0.015	-71.6	107.7	-1.25	1.88			
H1815 (D) MTH	169.1	-78.9	MAD 10.8	0	1	9	349.1	78.9	78.9	6.093	1.377	0	0	0	-20.4	014.9	68.6	-3.96	0.935	00.7	010.9	0.013	0.19			
							000.0	00.0	00.0	0	0	0	0	0	-20.4	014.9	00.0	0.00	0.326	69.7	014.9	1.216	0.259			
H18 summary:							000.0	00.0	00.0	0	0	0	0	0	-20.4	014.9	00.0	0.00	0.326	69.7	014.9	1.216	0.259			
green=steep mode							000.0	00.0	00.0	0	0	0	0	0	-20.4	014.9	00.0	0.00	0.326	69.7	014.9	1.216	0.259			
gold=pyrrhotite probs 525 Ma hydrothermal							000.0	00.0	00.0	0	0	0	0	0	-20.4	014.9	00.0	0.00	0.326	69.7	014.9	1.216	0.259			
orange=present field							000.0	00.0	00.0	0	0	0	0	0	-20.4	014.9	00.0	0.00	0.326	69.7	014.9	1.216	0.259			
blue=NWU, unknown age							000.0	00.0	00.0	0	0	0	0	0	-20.4	014.9	00.0	0.00	0.326	69.7	014.9	1.216	0.259			
pink=WNW-down unknown age							000.0	00.0	00.0	0	0	0	0	0	-20.4	014.9	00.0	0.00	0.326	69.7	014.9	1.216	0.259			
yellow=probs lightning (ChRM parallel to LN2)							000.0	00.0	00.0	0	0	0	0	0	-20.4	014.9	00.0	0.00	0.326	69.7	014.9	1.216	0.259			
							000.0	00.0	00.0	0	0	0	0	0	-20.4	014.9	00.0	0.00	0.326	69.7	014.9	1.216	0.259			
H1601 ATO	344.5	32.8	10.0	0	6	7	344.5	32.8	32.8	6.013	0.572	0	0	0	-20.4	014.9	17.9	-22.75	0.569	48.9	-007.9	0.853	-0.138			
H1602 HTO	255.3	-34.3	15.1	0	7	7	075.3	34.3	34.3	1.314	0.599	0	0	0	-20.4	014.9	18.8	67.13	0.362	06.5	082.0	0.113	1.431			
H1605 MTO square	200.8	62.2	13.9	0	5	7	200.8	62.2	62.2	3.505	1.086	0	0	0	-20.4	014.9	43.5	-32.19	0.384	-61.1	-017.3	-1.066	-0.303			
H1606 MTO,MEP	319.8	-76.8	10.8	1	6	8	139.8	76.8	76.8	2.44	1.34	-0.174	0.147	-0.97	-20.4	014.9	64.9	20.43	0.690	-38.2	035.3	-0.667	0.616	-0.619	0.641	0.4537
H1608 MTO,MEP	134.2	-61.9	9.5	0	11	11	314.2	61.9	61.9	5.484	1.08	0	0	0	-20.4	014.9	43.1	-32.61	0.767	13.9	-017.8	0.242	-0.31			
H1609 MTO	056.8	00.9	24.3	0	6	8	056.8	00.9	00.9	0.991	0.016	0	0	0	-20.4	014.9	00.5	76.70	0.185	30.7	091.6	0.536	1.598			
H1610 A-F (basemt exo)	358.3	-60.4	18.5	0	6	6	178.3	60.4	60.4	3.112	1.054	0	0	0	-20.4	014.9	41.4	3.55	0.336	-68.9	018.4	-1.203	0.321			
H1610 L-Q (basemt) MTO	243.6	-70.2	11.3	1	6	9	063.6	70.2	70.2	1.11	1.225	0.1506	0.303	-0.94	-20.4	014.9	54.2	31.59	0.798	-02.2	046.4	-0.039	0.811	-0.039	0.689	0.7242
H1611 MTO 8/8	184.1	-58.2	17.3	0	8	8	004.1	58.2	58.2	0.072	1.016	0	0	0	-20.4	014.9	38.9	3.71	0.805	30.6	018.6	0.535	0.324			
H1611 MTO 6/8	190.9	-48.8	13.4	0	6	8	010.9	48.8	48.8	0.19	0.852	0	0	0	-20.4	014.9	29.7	12.17	0.714	38.8	027.0	0.678	0.472			
H1612 MTO,MEP	096.6	-73.3	21.4	0	8	8	276.6	73.3	73.3	4.828	1.279	0	0	0	-20.4	014.9	59.0	-31.79	0.773	-14.0	-016.9	-0.245	-0.296			
H1612 (7/8; no big improvement)	077.9	-69.8	18.4	0	7	8	257.9	69.8	69.8	4.501	1.218	0	0	0	-20.4	014.9	53.7	-39.14	0.668	-23.4	-024.3	-0.408	-0.424			
							000.0	00.0	00.0	0	0	0	0	0	-20.4	014.9	00.0	0.00	0.326	69.7	014.9	1.216	0.259			
note: H1603.04.07 scat/lightning							000.0	00.0	00.0	0	0	0	0	0	-20.4	014.9	00.0	0.00	0.326	69.7	014.9	1.216	0.259			
also H1613-20 scat/low Tunbl							000.0	00.0	00.0	0	0	0	0	0	-20.4	014.9	00.0	0.00	0.326	69.7	014.9	1.216	0.259			
							000.0	00.0	00.0	0	0	0	0	0	-20.4	014.9	00.0	0.00	0.326	69.7	014.9	1.216	0.259			
							000.0	00.0	00.0	0	0	0	0	0	-20.4	014.9	00.0	0.00	0.326	69.7	014.9	1.216	0.259			
Expected directions							000.0	00.0	00.0	0	0	0	0	0	-20.4	014.9	00.0	0.00	0.326	69.7	014.9	1.216	0.259			
Meert+95 Mbozi	327.4	18.9					327.4	18.9	18.9	5.714	0.33	0	0	0	-20.4	014.9	09.7	-49.91	0.419	46.0	-035.1	0.804	-0.612			
Wingate+10 Luakela A	313.1	-01.7					133.1	01.7	01.7	2.323	0.03	0	0	0	-20.4	014.9	00.9	72.97	-0.210	-40.2	121.9	-0.702	2.127			
Wingate+10 Luakela B	049.6	-04.4					229.6	04.4	04.4	4.007	0.077	0	0	0	-20.4	014.9	02.2	-76.04	-0.177	-38.4	270.9	-0.669	4.728			
Moloto-A-Kenguemba+08 Nola 570	030.0	-45.9					210.0	45.9	45.9	3.665	0.801	0	0	0	-20.4	014.9	27.3	-69.94	0.152	-61.8	-055.1	-1.078	-0.961			
Meert+Voo 96 Sinyai metadol 547±4	260.0	57.2					260.0	57.2	57.2	4.538	0.998	0	0	0	-20.4	014.9	37.8	-55.89	0.494	-20.0	-041.0	-0.349	-0.716			
Trindade+06 Itabaiana pole rotd to Congo (30.6,	319.9	42.2					319.9	42.2	42.2	5.583	0.737	0	0	0	-20.4	014.9	24.4	-42.99	0.590	30.6	-028.1	0.535	-0.491			
PDF	000.0	-36.6					180.0	36.6	36.6	3.142	0.639	0	0	0	-20.4	014.9	20.4	0.00	0.000	-90.0	014.9	-1.57	0.259			
PLF	350.0	-63.0					170.0	63.0	63.0	2.967	1.1	0	0	0	-20.4	014.9	44.5	16.73	0.387	-64.5	031.6	-1.126	0.551			
							000.0	00.0	00.0	0	0	0	0	0	-20.4	014.9	00.0	0.00	0.326	69.7	014.9	1.216	0.259			
							000.0	00.0	00.0	0	0	0	0	0	-20.4	014.9	00.0	0.00	0.326	69.7	014.9	1.216	0.259			
Means:							000.0	00.0	00.0	0	0	0	0	0	-20.4	014.9	00.0	0.00	0.326	69.7	014.9	1.216	0.259			
Cm1-2: H1601,08,11; H1811pyr	341.2	51.1	20.2	0	4	site	341.2	51.1	51.1	5.955	0.892	0	0	0	-20.4	014.9	31.8	-19.50	0.725	34.8	-004.6	0.608	-0.081			
E-Cm1: H1605; H1807,10	218.5	57.7	18.4	0	3	site	218.5	57.7	57.7	3.814	1.007	0	0	0	-20.4	014.9	38.3	-52.98	0.345	-52.3	-038.1	-0.913	-0.665			
Steep: H1606,10M-Q; H1804-06,08,08,12	068.7	83.7	10.3	0	7	site	068.7	83.7	83.7	1.199	1.461	0	0	0	-20.4	014.9	77.5	12.03	0.884	-15.4	026.9	-0.269	0.469			
							000.0	00.0	00.0	0	0	0	0	0	-20.4	014.9	00.0	0.00	0.326	69.7	014.9	1.216	0.259			
							000.0	00.0	00.0	0	0	0	0	0	-20.4	014.9	00.0	0.00	0.326	69.7	014.9	1.216	0.259			
							000.0	00.0	00.0	0	0	0	0	0	-20.4	014.9	00.0	0.00	0.326	69.7	014.9	1.216	0.259			
							000.0	00.0	00.0	0	0	0	0	0	-20.4	014.9	00.0	0.00	0.326	69.7	014.9	1.216	0.259			
							000.0	00.0	00.0	0	0	0	0	0	-20.4	014.9	00.0	0.00	0.326	69.7	014.9	1.216	0.259			
							000.0	00.0	00.0	0	0	0	0	0	-20.4	014.9	00.0	0.00	0.326	69.7	014.9	1.216	0.259			
							000.0	00.0	00.0	0	0	0	0	0	-20.4	014.9	00.0	0.00	0.326	69.7	014.9	1.216	0.259			
							000.0	00.0	00.0	0	0	0	0	0	-20.4	014.9	00.0	0.00	0.326	69.7	014.9	1.216	0.259			
							000.0	00.0	00.0	0	0	0	0	0	-20.4	014.9	00.0	0.00	0.326	69.7	014.9	1.216	0.259			
							000.0	00.0	00.0	0	0	0	0	0	-20.4	014.9	00.0	0.00	0.326	69.7	014.9	1.216	0.259			
							000.0	00.0	00.0	0	0	0	0	0			00.0	#DIV/0!	0.000	90.0	#DIV/0!	1.571	#DIV/0!			
			R =	6.83					N =	7		0.2732	0.701	-6.79						R =	6.4	N =	7.0	-1.679	5.545	2.7679
			k =	35.1																K =	10.4					
			a95 =	10.3																A95 =	19.7					
																						-0.265	0.463			
Mean	068.7	83.7								1.199	1.46				-20.4	014.9	77.5		Mean pole	-15.2	026.5	(mean in radians)				
	248.7	-83.7								(mean in radians)																
																				-17.3	022.8	in thesis				

Table 1. This table provides a summary of the 35 sites of this study. The sites which yielded useful mean characteristic remnant directions are included as rows. The sites thought to provide the oldest and most comprehensive direction are averaged to determine a single pole direction. This corresponds to subset A.

DISCUSSION

After compiling average characteristic directions for the 35 sites, 21 quality-filtered sites were used in further analysis. These quality-filtered sites all have an α_{95} value of less than 18.5º. The directions, errors, and sample sizes of these sites are summarized in Table 1. None of these sites agree with the expected NW-shallow directions for the southern Congo at ca. 750 Ma, as projected in local coordinates from previously published paleomagnetic poles in the eastern side of the craton, including the Mbozi complex of Tanzania (Meert et al. 1995) and the Luakela volcanics of Zambia (Wingate et al. 2010). Figure 3 is a summary equal-area stereoplot of all 21 quality-filtered site-mean characteristic remanent magnetizations (ChRMs). Six sites with ChRM directions similar to either the Present Dipole Field (PDF) or Present Local Field (PLF) at the sampling region are shown in Figure 4A with their likely overprint directions. Both sites represent recent overprinting and are excluded from future analyses.

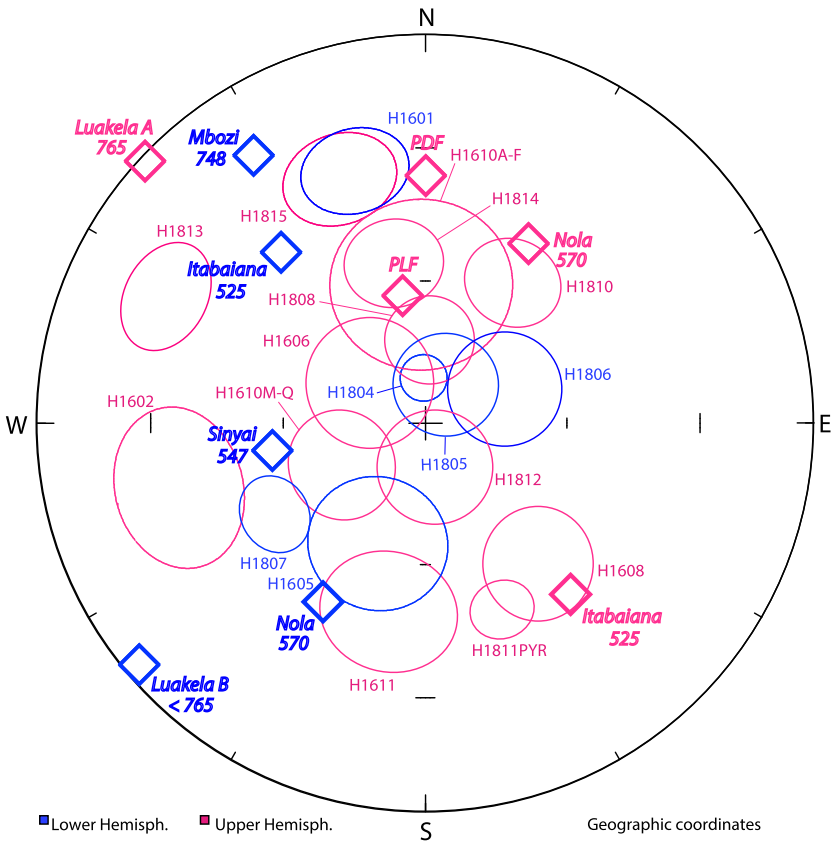

Figure 3. This stereonet summarizes the directions of the 21 quality-filtered ChRMs. The ellipses represent the directions and are labeled with their site name. The diamonds are previous paleomagnetic poles. They are labeled with the age in Ma and the name of the formation of study.

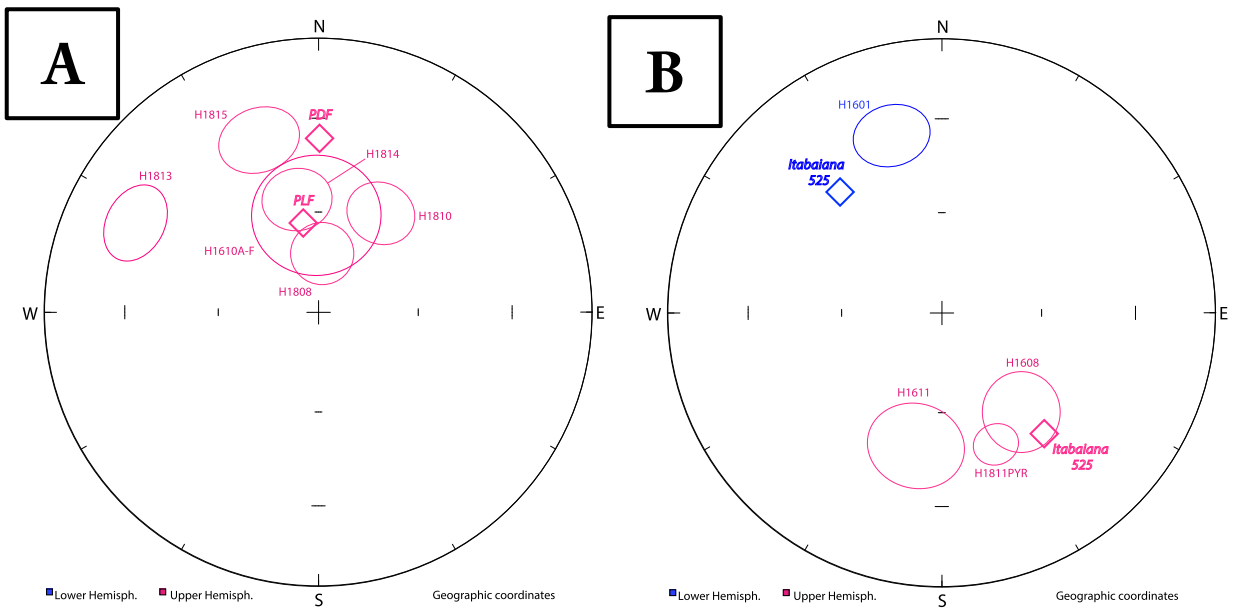

Figure 4. A. These 6 site means are directions which coincide with the current present field such that they are thought to be the result of remagnetization. **B.** This dual-polarity diagram shows the 4 site means associated with the Itabiana pole of the Congo craton. This pole has been transformed from its published direction to the south Congo.

Four sites with a dual-polarity grouping of directions similar to the expected directions from the end of Early Cambrian time (as represented by the Itabaiana Dykes direction of Trindade et al. (2006) rotated to African coordinates from Brazil) are shown in Figure 4B. This component, named Subset C, is associated at one site with visible sulfide mineralization in the samples, and is considered to represent hydrothermal alteration in the waning stages of the Damara orogeny (Pirajno and Jacob 1991).

Of the remaining 11 site-mean ChRMs, one (H1602) carries a low-inclination hematitic direction that is in the vicinity of that expected from the secondary "B" component of the Luakela Volcanics in Zambia (Wingate et al., 2010). The Luakela-B component is specifically associated with secondary hematite alteration. The other 10 sites show dual-polarity and have a streaked distribution between nearly vertical directions and SW-down / NE-up. The latter direction, isolated in three sites and named Subset B, would be expected from a mid-Ediacaran overprint, as

represented by the ca. 570-Ma pole from the Nola metadolerite dykes in Central African Republic (Moloto-A-Kenguemba et al., 2008). The other edge of the streaked distribution, nearly vertical ChRMs in both polarities, may be slightly older or younger than ca. 570 Ma, as would be expected if Congo craton drifted between moderate and steep paleolatitudes during protracted remagnetization. The Congo apparent polar wander (APW) path is well defined from 570 Ma (Nola dykes, ibid.) to ca. 550 Ma (Sinyai metadolerite of Tanzania; Meert and Van der Voo, 1996), and younger through the Early Cambrian (Mitchell et al., 2010), without traversing the pole at any time during that interval. Therefore, the very steep directions at the far end of the streaked distribution is considered to be slightly older than 570 Ma, and named Subset A.

While exact age of Subset A is unknown, it is likely that its seven steep sites represent an Early- to Mid-Ediacaran overprint, perhaps 600-580 Ma. Three factors support an overprint interpretation for the steep Subset A component. The polar latitude implied by the pole is in contrast with the carbonate platform developed on the Congo craton ca. 750 Ma. This carbonate platform (Hoffman and Halverson, 2008) would require warm waters to be deposited, conditions which are much more likely in the tropics. It is notably distinct from previously reported ca. 750 Ma Congo poles, as noted above, and the Subset A direction is observed in both the dykes and basement, thus suggesting a regionally widespread thermochemical overprint. An age of at least ca. 580 Ma would allow the craton to move from the pole and remain in agreement with the previously published APW path.

Figure 5 summarizes the current interpretation of the polar wander path of the Congo craton from 570 Ma to late Paleozoic time, and includes the two previously reported poles from ca. 750 Ma (Luakela-A and Mbozi). As discussed above, various subsets of data appear to

correspond to Ediacaran-Cambrian poles of appropriate age for overprinting by hydrothermal alteration of the Damara orogeny. Neither of our two baked contact tests yielded a positive result; and in one test, the basement rocks yielded a steep direction interpreted as one of the overprinted subsets.

The significant presumed Ediacaran-Cambrian subsets have poles in three different locations. The youngest two B and C, agree with other published poles for the Congo craton. The C subset, the youngest, contains 6 sites and is likely showing the same direction of magnetization as the Itabaiana pole (Trindade 2006). This would give this direction an age of ca. 525 Ma which is from the mafic Itabaiana dykes from the north-western area of the Congo–São Francisco craton (Trindade 2006). A paleomagnetic pole calculated from the 7 steepest sites, subset A, suggests a

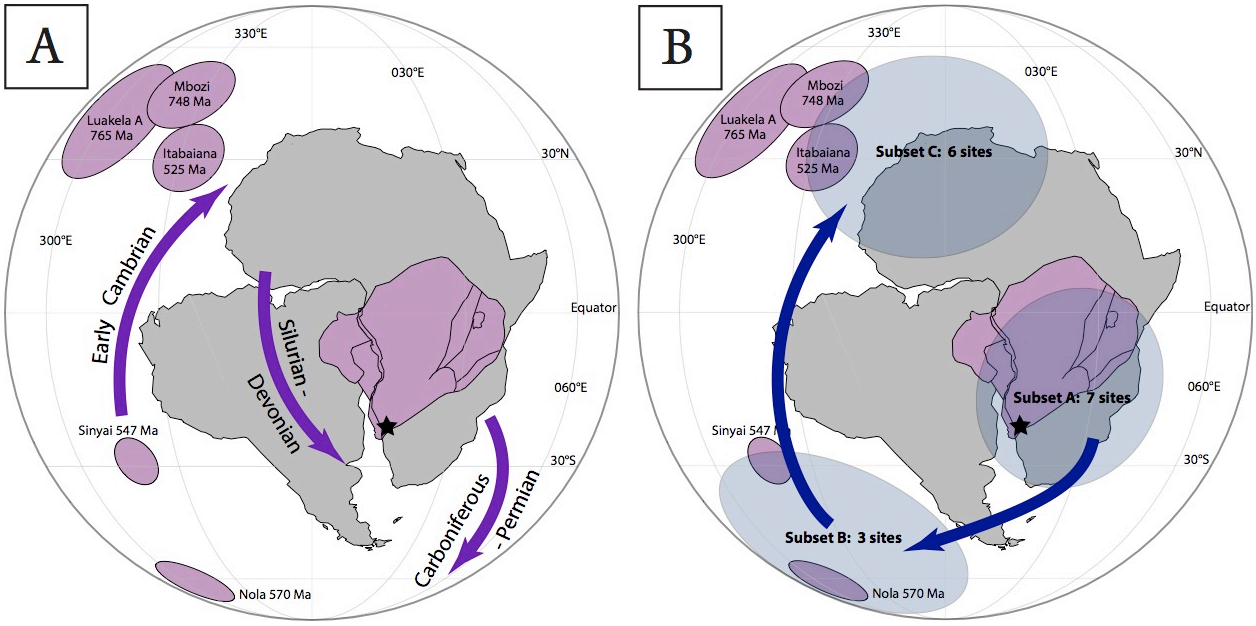

Figure 5. A. The lavender ellipses show published poles and their ages for the region of interest. The study area is represented by a black star on the lavender Congo craton. The purple arrows show a likely APWP for the south pole for the site from Early Cambrian until the present. **B.** The data from this study are shown in three subsets, A thought to be oldest and C youngest. The navy arrows summarize the proposed new APW path.

polar excursion of the craton in mid-Ediacaran time. This excursion, while unlikely ca. 750 Ma, is

possible later in the history of the craton. Based on the APWP from [CITE] of the Congo craton, this pole is likely from ca. 580 Ma.

CONCLUSIONS & FURTHER WORK

The dykes of the Oas syenite in northern Namibia show complete overprinting and no original magnetization can be determined from the samples collected in 2016 or 2018. A previously unknown pole and new APW path of for the craton is proposed. However, an upper age constraint be confirmed with the current data. This polar excursion implies a much larger separation between the Congo and Kalahari cratons than argued by Gray *et al.* 2008. The closure of this wide basin and the accompanying Damara Orogen are possibly responsible for the regional remagnetization of these dykes. Given the extensive overprinting and remagnetization across the northern Damara foreland, this region proves unlikely to yield primary Precambrian poles. A greater distance from the margin could result in samples less influenced by the remagnetization of the action of the orogen. Further study and more precise constraints about the closure of this basin may be found through paleomagnetic investigation of the northern Kalahari craton; while more information about the location of the Congo craton

WORKS CITED

Buchan K.L. Baked Contact Test. In: Gubbins D., Herrero-Bervera E. (eds) *Encyclopedia of Geomagnetism and Paleomagnetism.* Springer, Dordrecht (2007)

Evans, D.A.D. Personal Communication. (2019).

Evans, D.A.D., *et al.* "Return to Rodinia? Moderate to high palaeolatitude of the São Francisco/Congo craton at 920 Ma." *Geological Society, London, Special Publications* 424.1 (2016): 167-190

Frets, Dirk Cornelis. *Geology and structure of the Huab-Welwitschia area, South West Africa*. University of Cape Town, Department of Geology, 1969.

Gray, David R., *et al.* "A Damara orogen perspective on the assembly of southwestern Gondwana." *Geological Society, London, Special Publications* 294.1 (2008): 257-278.

Hoffman, P.F., *et al.* "Precise U-Pb zircon ages for early Damaran magmatism in the Summas Mountains and Welwitschia Inlier, northern Damara belt, Namibia." *Communications of the geological survey of Namibia* 11 (1996): 47-52.

Hoffman, P., and G. Halverson. "Otvi Group of the Western Northern Platform, the Eastern Kaoko Zone and the Western Northern Margin Zone." Namibia, 2008.

Hoffman, P. F. "Strange bedfellows: glacial diamictite and cap carbonate from the Marinoan (635 Ma) glaciation in Namibia." *Sedimentology* 58.1 (2011): 57-119.

Jones, C. H., User-driven Integrated Software Lives: "PaleoMag" Paleomagnetics Analysis on the Macintosh, Computers and Geosciences, 28 (10), 1145-1151, 2002.

Jung, S., E. Hoffer, and S. Hoernes. "Neo-Proterozoic rift-related syenites (Northern Damara Belt, Namibia): geochemical and Nd–Sr–Pb–O isotope constraints for mantle sources and petrogenesis." *Lithos* 96.3-4 (2007): 415-435.

Meert, Joseph G., Rob van der Voo, and Samwel Ayub. "Paleomagnetic investigation of the Neoproterozoic Gagwe lavas and Mbozi complex, Tanzania and the assembly of Gondwana." *Precambrian Research* 74.4 (1995): 225-244.

Meert, Joseph G. "Strange attractors, spiritual interlopers and lonely wanderers: the search for pre-Pangean supercontinents." *Geoscience Frontiers* 5.2 (2014): 155-166.

Merdith, Andrew S., *et al.* "A full-plate global reconstruction of the Neoproterozoic." *Gondwana Research* 50 (2017): 84-134.

Mitchell, Ross N., Taylor M. Kilian, and David A.D. Evans. "Supercontinent cycles and the calculation of absolute palaeolongitude in deep time." *Nature* 482.7384 (2012): 208.

Moloto-A-Kenguemba, Gaétan R., et al. "A late Neoproterozoic paleomagnetic pole for the Congo craton: Tectonic setting, paleomagnetism and geochronology of the Nola dike swarm (Central African Republic)." *Precambrian Research* 164.3-4 (2008): 214-226

Pirajno, F., and R. E. Jacob. "Gold mineralisation in the intracontinental branch of the Damara Orogen, Namibia: a preliminary survey." *Journal of African Earth Sciences (and the Middle East)* 13.3-4 (1991): 305-311.

Salminen, Johanna, et al. "Direct Mesoproterozoic connection of the Congo and Kalahari cratons in proto-Africa: Strange attractors across supercontinental cycles." *Geology* 46.11 (2018): 1011-1014.

Trindade, Ricardo IF, et al. "Paleomagnetism of Early Cambrian Itabaiana mafic dikes (NE Brazil) and the final assembly of Gondwana." *Earth and Planetary Science Letters* 244.1-2 (2006): 361-377.

Wingate, Michael TD, Sergei A. Pisarevsky, and Bert De Waele. "Paleomagnetism of the 765 Ma Luakela volcanics in Northwest Zambia and implications for Neoproterozoic positions of the Congo Craton." *American Journal of Science* 310.10 (2010): 1333-1344.